ORNL/TM--8319

DE82 019727

DISCLAIMER

This report was prepared as an account of work sponsored by an agency of the United States Government. Neither the United States Government nor any agency thereof, nor any of their employees, makes any warranty, express or implied, or assumes any legal liability or responsibility for the accuracy, completeness, or usefulness of any information, apparatus, product, or process disclosed, or represents that its use would not infringe privately owned rights. Reference herein to any specific commercial product, process, or service by trade name, trademark, manufacturer, or otherwise, does not necessarily constitute or imply its endorsement, recommendation, or favoring by the United States Government or any agency thereof. The views and opinions of authors expressed herein do not necessarily state or reflect those of the United States Government or any agency thereof.

ORNL/TM-8319
Dist. Category UC-20a,d,g

Contract No. W-7405-eng-26

FUSION ENERGY DIVISION

RF-ASSISTED CURRENT STARTUP IN THE FUSION ENGINEERING DEVICE (FED)

S. K. Borowski*
Y-K. M. Peng
T. Kammash*

NOTICE This document contains information of a preliminary nature. It is subject to revision or correction and therefore does not represent a final report.

Date Published - August 1982

*University of Michigan, Ann Arbor, Michigan

Prepared by the
OAK RIDGE NATIONAL LABORATORY
Oak Ridge, Tennessee 37830
operated by
UNION CARBIDE CORPORATION
for the
DEPARTMENT OF ENERGY

DISTRIBUTION OF THIS DOCUMENT IS UNLIMITED

CONTENTS

ABSTRACT 1

1. INTRODUCTION 2
2. PHYSICS DISCUSSION OF WAVE-PLASMA INTERACTIONS 3
   2.1 EXTRAORDINARY WAVE ABSORPTION AT THE UHR LAYER 3
   2.2 REGION OF MICROWAVE POWER DEPOSITION 5
3. AMBIPOLAR POTENTIAL AND ITS EFFECTS ON TRANSPORT 6
   3.1 ESTIMATING THE AMBIPOLAR POTENTIAL 6
   3.2 ENERGY TRANSPORT TO THE LIMITER 11
   3.3 EFFECTS OF AMBIPOLAR ELECTRIC FIELD ON PARTICLE CONFINEMENT 12
4. PARTICLE AND ENERGY TRANSPORT PRIOR TO CURRENT INITIATION 14
   4.1 PARTICLE BALANCE 14
   4.2 ENERGY BALANCE 15
   4.3 ELECTRON PREHEATING ASSUMPTIONS 16
   4.4 TRANSPORT REGIMES OF INTEREST 18
5. COMPARISON WITH ISX-B EXPERIMENTAL RESULTS 19
   5.1 THEORY VS EXPERIMENT 21
      5.1.1 Effect of Error Fields 22
      5.1.2 Secondary Electron Emission 22
      5.1.3 Evidence of Higher Electron Temperatures 25
6. APPLICATION TO THE FED TOKAMAK 27
7. CURRENT INITIATION AND RAMP-UP 30
   7.1 EXPANDING PLASMA OPTIONS 33
8. START-UP VOLTAGE AND VOLT-SECOND REQUIREMENTS 36
   8.1 ELECTRON TEMPERATURE ESTIMATES DURING CURRENT STARTUP ... 36
   8.2 CALCULATING THE APPLIED LOOP VOLTAGE AND ITS COMPONENTS . 38
   8.3 RESULTS AND DISCUSSION 40
9. SUMMARY 49

ACKNOWLEDGMENTS 50

REFERENCES 51

ABSTRACT

Auxiliary rf heating of electrons before and during the current rise phase in the Fusion Engineering Device is examined as a means of reducing both the initiation loop voltage and resistive flux expenditure during startup. Prior to current initiation 1 to 2 MW of electron cyclotron resonance heating (ECRH) power at $\sim$90 GHz is used to create a small volume of high conductivity plasma ($T_e \simeq 100$ eV, $n_e \simeq 10^{13}$ cm^{-3}) near the upper hybrid resonance (UHR) region. This plasma conditioning permits a small radius ($a_o \simeq 0.2$-0.4 m) current channel to be established with a relatively low initial loop voltage ($\lesssim 25$ V). During the subsequent plasma expansion and current ramp phase, additional rf power is introduced to reduce volt-second consumption due to plasma resistance. A near classical particle and energy transport model has been developed to estimate the efficiency of electron heating in a currentless toroidal plasma. The model assumes that preferential electron heating at the UHR leads to the formation of an ambipolar sheath potential between the neutral plasma and the conducting vacuum vessel and limiter. The ambipolar electric field (E_{AMB}) enables the plasma to neutralize itself via poloidal $\vec{E}_{AMB} \times \vec{B}$ drift. This form of effective rotational transform "short-circuits" the vertical charge separation and improves particle confinement. The benefits of this effective electrostatic confinement are tempered, however, by the possibility of significant secondary electron emission from the limiters and vessel wall. Reasonably good agreement has been found between our theoretical estimates and the measurements made during ECR preheating experiments on the ISX-B tokamak. This agreement provides some confidence in the preheating power and startup loop voltage estimates obtained for the FED.

1. INTRODUCTION

Considerable interest presently exists in the use of electron cyclotron resonance heating (ECRH) power to assist current startup in large tokamak plasmas such as the Fusion Engineering Device (FED).[1] The primary motivation for considering rf preionization and currentless electron heating (preheating) is the potential for significantly reducing the initiation loop voltage and resistive flux loss during startup.[2] These reductions can simplify the engineering design of the ohmic heating system and substantially increase the pulse length capability of FED.

To date, our FED studies have focussed on a rf-assisted, expanding radius startup consisting of three separate phases:

1. Extraordinary mode waves are first injected from the torus high field side producing ionization and electron heating near the UHR layer before current initiation. The UHR layer, which is limited in volume, is deliberately positioned near the outboard side of the chamber to facilitate a small radius current startup. Away from the UHR layer, a low temperature (a few eV) partially ionized plasma, produced by nonresonant rf breakdown of the prefill gas, is expected to fill the chamber.

2. While maintaining ECRH a low loop voltage is applied which induces a plasma current in the preheated region. Current initiation occurs over a relatively long time scale (0.2-0.3 s) to avoid the formation of plasma skin currents. The initial current channel is limited to $\lesssim$0.4 m in minor radius by a startup limiter located at the outboard midplane. This size is maintained until the safety factor q_I reaches a desired value.

3. Additional supplementary heating [either ECRH or proton minority heating (ICRF)] is then introduced as the minor radius and plasma current are increased while holding $q_I = 2.4$ ($q_\psi = 3.2$) and compressing the plasma major radius. This supplementary

heating minimizes the resistive loss of volt-seconds and allows a relatively slow current ramp-up during the remainder of the current start-up phase.

In the following sections we examine the physics and plasma engineering issues associated with each of these phases. Covered in Sect. 2 is a review of the wave-plasma interactions during UHR absorption. The location of the rf power deposition and the selection of the required microwave frequency are also discussed. Formation of an ambipolar sheath potential and its effects on plasma transport are discussed in Sect. 3. With this as a basis, Sect. 4 presents global particle and energy balance equations describing the ambipolar loss of electrons and ions from a currentless toroidal plasma. A comparison between theory and experiment is found in Sect. 5, where model predictions are shown to provide a plausible interpretation of the recent ISX-B observations. In Sect. 6 the UHR heating model is used to predict the power requirements for FED under a variety of preheating conditions. Current startup and minor radius expansion are discussed in Sect. 7. The details of the equations used for determining the electron temperature and plasma loop voltage during current rise are presented in Sect. 8. Also shown in this section is the sensitivity of the voltage and flux requirements to variations in the initial minor radius, oxygen impurity content, and electron preheating level. Our findings regarding rf-assisted current startup are summarized in Sect. 9.

2. PHYSICS DISCUSSION OF WAVE-PLASMA INTERACTIONS

2.1 EXTRAORDINARY WAVE ABSORPTION AT THE UHR LAYER

During the preheating phase, fundamental electron cyclotron resonance heating is injected from the high field side of the torus as extraordinary mode (EO) radiation. As the ECRH power preionizes the initial fill gas, two types of wave-plasma interactions are observed.[3] During the early stages of rf heating, the electron density is low, and strong cyclotron absorption of the EO-wave results from a resonant energy transfer from

the right-circularly polarized component of the wave to the gyrating electrons. As the density increases, however, the EO-wave becomes left-circularly polarized and can no longer accelerate electrons at the cyclotron resonance.[4] For finite temperature plasmas, the transition from the low-to-high-density regime occurs when[5]

$$\alpha \equiv \frac{(\omega_{pe})^2}{(\omega_{RF})^2} \gtrsim \left(\frac{kT_e}{m_e c^2}\right)^{1/2} \cos\theta \ . \tag{2.1}$$

Here ω_{pe} is the electron plasma frequency, ω_{RF} $(=2\pi f_{RF})$ is the applied microwave frequency, and θ is the angle between the propagation vector $\vec{k}$ and the direction of the toroidal magnetic field at the plasma edge.

When Eq. (2.1) is satisfied, the cyclotron resonance layer becomes transparent to the EO-wave, and strong wave absorption can then occur near the UHR layer where

$$(\omega_{RF})^2 = (\omega_{UH})^2 \equiv (\omega_{pe})^2 + (\omega_{ce})^2 \ , \tag{2.2}$$

ω_{ce} being the electron cyclotron frequency. Nearing the UHR layer, the almost undamped EO-wave can undergo nonlinear parametric decay into electron Bernstein and ion-acoustic modes.[6] The high frequency Bernstein waves subsequently transfer their energy to the plasma electrons via Landau damping when $\vec{k} \cdot \vec{B}$ is finite.[7] This strong damping can heat electrons to temperatures ranging from 50-200 eV.[8,3]

The absorption of extraordinary waves by electrons near the UHR region is an attractive heating process, because the wave energy is efficiently transferred to the bulk electrons in a small volume. Sufficient experimental evidence exists to warrant our studies of this heating technique. Experimental studies by Anisimov et al.[3] indicated the feasibility of UHR absorption by a plasma in a purely toroidal magnetic field, but only for short rf pulse lengths (<1 ms). Recently, longer pulse ($\lesssim$15 ms) preionization experiments on the much larger ISX-B

tokamak[8,9] have also confirmed UHR absorption and heating using time-resolved density measurements, temperature diagnostics and high-speed photography to examine the plasma characteristics during preheating.

2.2 REGION OF MICROWAVE POWER DEPOSITION

In FED the UHR layer is positioned at $R_{UH} = 5.9$ m, a location which facilitates the growth of a small radius plasma ($a_o \simeq 0.2$ m) off of a fixed outboard limiter during current initiation. As the plasma density builds during the preheating phase, the electron cyclotron resonance (ECR) and UHR layers become spatially separated by a distance ΔR given by

$$\Delta R = R_{UH} - R_{EC} = R_{EC}\left(\frac{1}{\sqrt{1-\alpha}} - 1\right) , \tag{2.3}$$

where

$$\alpha \equiv \frac{(\omega_{pe})^2}{(\omega_{RF})^2} = 1.03 \times 10^{-19} \left(\frac{n_e(m^{-3})[R_{EC}(m)]^2}{\left\{[B(R_o)(T)][R_o(m)]\right\}^2}\right) . \tag{2.4}$$

With $n_e \simeq 10^{19}$ m^{-3} (at the end of preheating), $R_{UH} = 5.9$ m and a toroidal field on axis of $B(R_o = 4.8\ m) = 3.62$ T, Eqs. (2.3) and (2.4) indicate that $R_{EC} = 5.58$ m and $\Delta R \simeq 0.32$ m. This implies a resonant microwave frequency requirement of $f_{RF} = 87$ GHz [f_{RF}(GHz) = 28 B_{EC}(T)]. For $a_o \simeq$ 0.4 m (PLT-size plasma), $R_{UH} = 5.7$ m, and the same electron density, one obtains $R_{EC} = 5.41$ m, $\Delta R \simeq 0.29$ m, and $f_{RF} = 90$ GHz. The expected thickness (Δ_H) of the heated UHR layer is discussed in Sect. 4.3.

3. AMBIPOLAR POTENTIAL AND ITS EFFECTS ON TRANSPORT

The preferential heating of electrons during the microwave pulse is expected to lead to enhanced electron transport and the spontaneous appearance of an ambipolar sheath electric field ($\vec{E}_{AMB}$) between the neutral plasma and the conducting vacuum vessel. The process of UHR heating and plasma sheath formation is depicted in Fig. 1. This generalized schematic shows a currentless tokamak plasma bounded by a continuous conducting poloidal limiter and vacuum vessel. The limiter and vessel walls are assumed to be electrically connected and to have a negative potential with respect to the plasma surface. The usually expected charge separation[10] is eliminated through the use of conducting limiters and walls and the formation of an ambipolar sheath. These effects reduce the buildup of a large vertical electric field.[11] Those electrons with energies below the ambipolar potential energy ($e\phi_{AMB}$) are confined by poloidal $\vec{E}_{AMB} \times \vec{B}$ drift. This effective rotational transform prevents a buildup of negative charge near the top of the vacuum vessel and enables the plasma to neutralize itself.

3.1 ESTIMATING THE AMBIPOLAR POTENTIAL[a]

In a currentless toroidal plasma, the principal loss mechanisms are assumed to be toroidal magnetic drift, V_D, and parallel drift, V_δ, resulting from small, stray error fields, δB, in the poloidal direction. The particle drift velocities and their associated lifetimes are given by

$$V_{Dj} = V_R + V_{\vec{\nabla}B} = \frac{cm_j}{e_j BR}\left(v_{\parallel j}^2 + \frac{v_{\perp j}^2}{2}\right) ,$$

$$V_{Dj} \simeq \frac{2ckT_j}{e_j BR} , \quad \tau_{Dj} = \frac{b}{V_{Dj}} \simeq \frac{bRB}{2 \times 10^8 \, T_j} , \tag{3.1}$$

[a]In this section, cgs units are used, and temperatures are given in electron volts.

ORNL-DWG 80-2189R FED

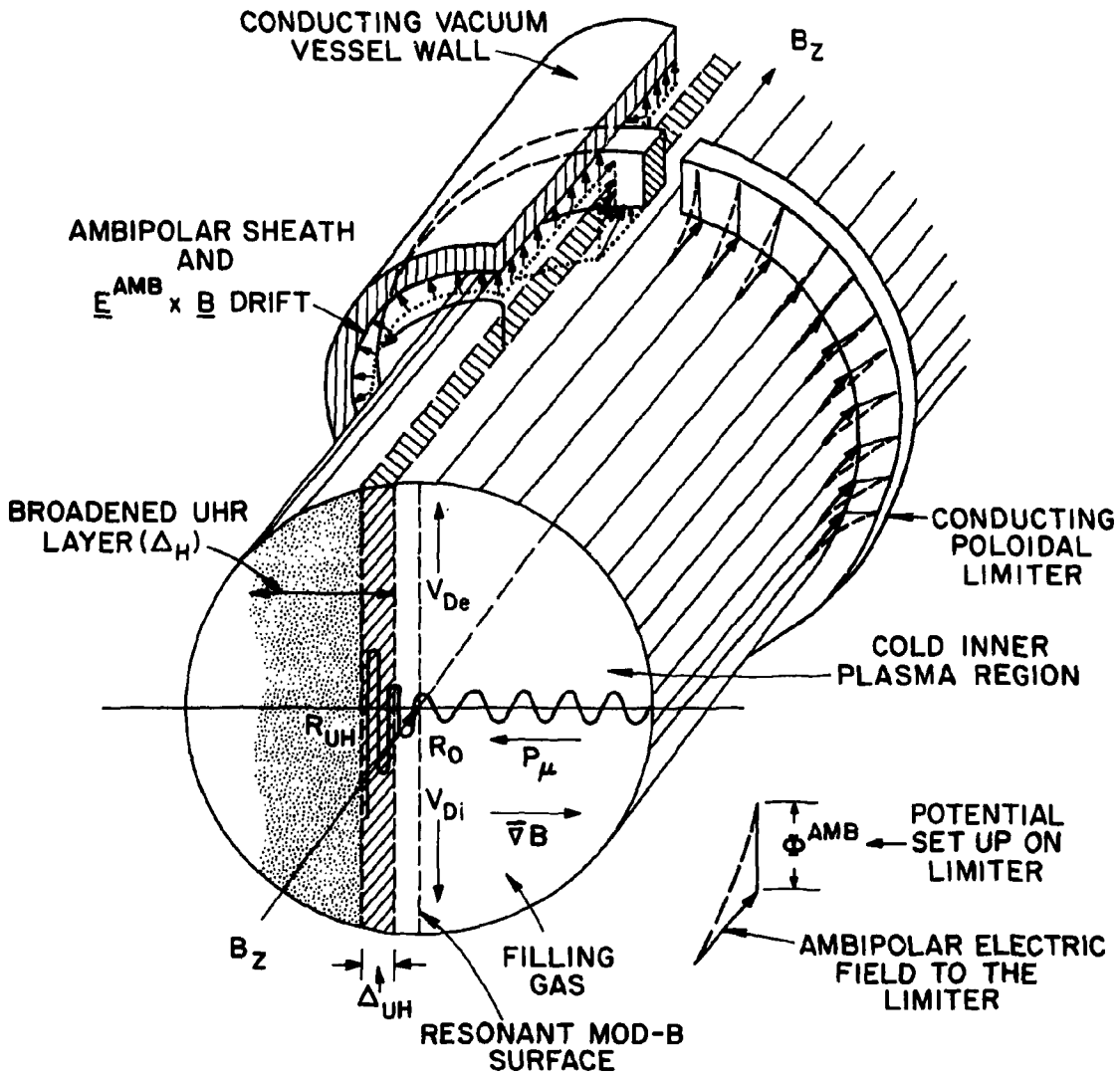

Fig. 1. Representation of electron preheating near the UHR region prior to current initiation.

$$V_{\delta j} = V_{\parallel j}\left(\frac{\delta B}{B}\right) \ , \ \tau_{\delta j} = \frac{b}{V_{\delta j}} = \frac{b}{V_{\parallel j}}\left(\frac{B}{\delta B}\right) \ , \tag{3.2}$$

where

$$V_{\parallel j} = \left(\frac{2kT_j}{\pi\ m_j}\right)^{1/2} \ ; \ j = e,i$$

is the average particle velocity along the direction of the magnetic field and 2b is the vertical height of the vacuum vessel.

In response to the predominant loss of heated electrons, an ambipolar potential develops which allows only a fraction of the drifting electrons $[\sim\exp(|e|\phi_{AMB}/kT_e)]$ to escape to the limiter or vacuum vessel wall. The magnitude of this potential adjusts itself automatically so as to ensure that the electron and ion loss rates are equal. In a device like ISX-B (Fig. 2a), all ions are lost once they drift into the limiter shadow (see Sect. 3.3). Because our UHR heating model is zero-dimensional and utilizes flat density and temperature profiles, the conventional ambipolarity constraint $[\vec{\nabla} \cdot (\vec{\Gamma}_e - \vec{\Gamma}_i) = 0]$ is replaced by the global "zero net current" condition

$$\sum_{k=C}^{H} \dot{N}_{ik} = \sum_{k=C}^{H} \dot{N}_{ek}(1 - \delta_k) \ , \tag{3.3}$$

where

$$\dot{N}_{ik} = n_{ik}\left(\frac{1}{\tau_{Di}} + \frac{1}{\tau_{\delta i}}\right)_k V_k \ , \tag{3.4}$$

and

$$\dot{N}_{ek} = n_{ek}\left(\frac{1}{\tau_{De}} + \frac{1}{\tau_{\delta e}}\right)_k \exp\left\{\frac{|e|\phi_{AMB}}{kT_{ek}}\right\} V_k \ . \tag{3.5}$$

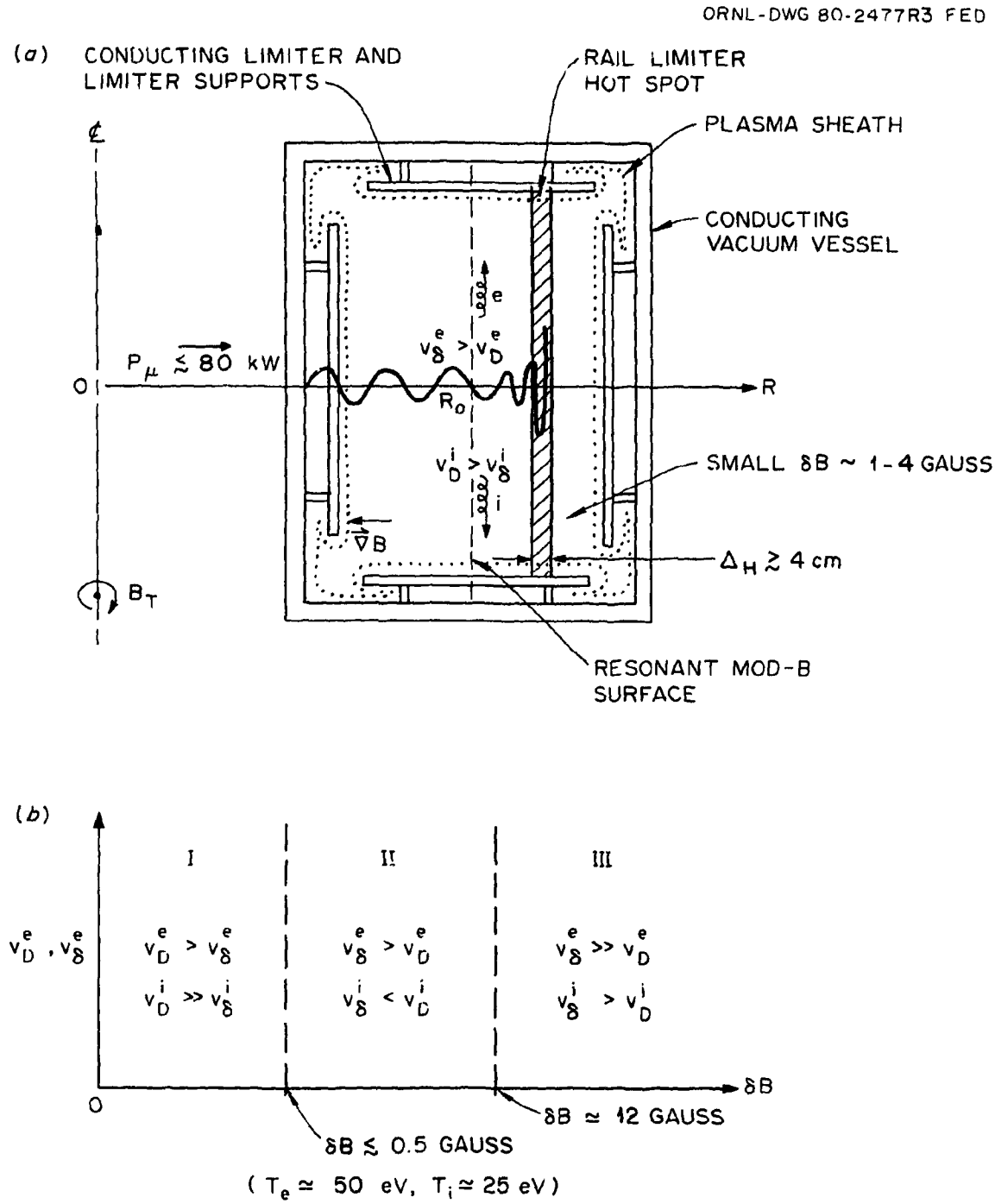

Fig. 2. Sketch showing (a) the ISX-B experimental configuration and (b) the various transport regimes for electrons and ions as a function of error field magnitude.

The parameters δ and V are the coefficients for secondary electron emission from the limiter surface (electrons/electron)[12] and the plasma volume, respectively; C and H refer to the cold (bulk) and hot (UHR layer) components of the preheated plasma. Considering for the moment only the hot plasma component and assuming quasi-neutrality in the interior plasma ($n_{eH} = n_{iH} = n$), the ambipolar potential is given by

$$\phi_{AMB} = \frac{-kT_{eH}}{|e|} \ln \left\{ (1 - \delta_H) \left[\frac{V_{De} + V_{\delta e}}{V_{Di} + V_{\delta i}} \right] \right\} \quad . \tag{3.6}$$

Equations (3.1) and (3.2) are used to write ϕ_{AMB} in terms of the appropriate drift velocities. As is evident in Eq. (3.6), the magnitude of ϕ_{AMB} will depend on the level of secondary electron emission and on whether transport is dominated by error field or curvature drift losses. To illustrate this sensitivity we consider two limiting cases. Assuming negligible error fields ($\delta B \approx 0$), the ambipolar potential reduces to

$$\phi_{AMB} = - \frac{kT_{eH}}{|e|} \ln \left\{ (1 - \delta_H) \frac{T_{eH}}{T_{iH}} \right\} \; ; \quad (V_D >> V_\delta) \; . \tag{3.7}$$

In the opposite extreme of large error fields, one obtains

$$\phi_{AMB} = \frac{-kT_{eH}}{2|e|} \ln \left\{ (1 - \delta_H)^2 \frac{m_i T_{eH}}{m_e T_{iH}} \right\} \; ; \quad (V_\delta >> V_D) \; . \tag{3.8}$$

This result is equivalent to that recovered when one considers plasma transport along magnetic field lines. Because of their higher thermal velocity, error fields allow the electrons to quickly spiral out of the vacuum chamber leading to large potential values.

As will be shown in Sect. 5, secondary electron effects are essential for explaining the preheating results in ISX-B. Emitted by primary particle bombardment with the limiter, secondary electrons reduce the sheath potential and subsequently lessen the effectiveness of the electrostatic confinement. Following sheath acceleration and return to

the interior plasma via $\vec{E}_{AMB} \times \vec{B}$ drift, these electrons can also cause additional cooling by thermalization with the hot electrons.

3.2 ENERGY TRANSPORT TO THE LIMITER

During preheating a significant percentage of electrons have energies below $e\phi_{AMB}$. These confined electrons are reflected from the presheath and returned to the plasma without a change in their energy. The energetic tail electrons with energies greater than $e\phi_{AMB}$ can penetrate this potential barrier, however. These lost electrons carry part of their energy directly to the limiter ($3/2kT_e$). The remainder supplies the energy needed to sustain the sheath against losses resulting from the inward acceleration of the cooler ions ($e\phi_{AMB}$). With experimental evidence[3,8] supporting a relatively uniform density and temperature in the heating regions, the total electron and ion power transported to the limiter is estimated to be

$$\sum_{k=C}^{H} (P_{TR})^k = \sum_{k=C}^{H} \frac{3}{2} kT_{ek}\dot{N}_{ek} + \left\{\frac{3}{2} kT_{ik} + e\phi_{AMB}\right\} \dot{N}_{ik} \ . \tag{3.9}$$

By using Eq. (3.3) a simplified form of Eq. (3.9) can be written as

$$\sum_{k=C}^{H} (P_{TR})^k = \sum_{k=C}^{H} \left[\left\{\underbrace{\frac{3}{2} + \frac{e\phi_{AMB}}{kT_{ek}} (1 - \delta_k)}_{\equiv \gamma_k}\right\} kT_{ek}\right] \dot{N}_{ek} + \frac{3}{2} kT_{ik}\dot{N}_{ik} . \tag{3.10}$$

Here, the parameter γ is defined as the electron energy coefficient and the quantity γkT_e represents the average energy transported from the interior plasma by each primary electron in the presence of secondary electron emission. Finally, if we consider only the hot plasma component in our analysis, the ambipolarity criteria of Eq. (3.3) reduces to[12]

$$\dot{N}_{iH} = \dot{N}_{eH} - \dot{N}_{2e} = \dot{N}_{eH}(1 - \delta_H) \ , \tag{3.11}$$

and we obtain the following compact expression for total transport power:

$$P_{TR}^{H} = \left\{ \gamma kT_{eH} + \frac{3}{2} kT_{iH} \right\} \dot{N}_{iH} \ , \tag{3.12}$$

where

$$\gamma \equiv \left\{ \frac{3/2}{(1 - \delta_H)} + \frac{e\phi_{AMB}}{kT_{eH}} \right\} \ . \tag{3.13}$$

3.3 EFFECTS OF AMBIPOLAR ELECTRIC FIELD ON PARTICLE CONFINEMENT

The ISX-B tokamak (Fig. 3) has upper and lower rail limiters which intercept all vertically drifting electrons and ions. The diameter of the rail limiter ($\Delta_L \gtrsim 3$ cm) is many times larger than the average toroidal drift distance of either the electrons ($\lesssim 0.1$ cm) or ions ($\lesssim 0.4$ cm) in the limiter shadow (~ 5 cm). These distances of vertical drift are, in turn, expected to be significantly larger than the thickness of the ambipolar sheath ($\Delta_s \gtrsim$ several Debye lengths). This comparison of scale lengths indicates appreciable interaction of both particle species with the ISX-B limiters. As illustrated in Fig. 3, the majority of ions reach the limiter while in the limiter shadow where $\vec{E}_{AMB}$ is nearly parallel to $\vec{B}$. The electrons, however, experience several possible electron-limiter interactions. Those heated electrons which just miss the limiter may undergo some poloidal deflection. The majority, however, drift along the sheath potential in the limiter shadow until they reach the conducting vessel wall; there, they experience poloidal $\vec{E}_{AMB} \times \vec{B}$ drift which effectively increases their confinement time. Only the energetic electrons, whose energy of motion toward the limiter exceeds $e\phi_{AMB}$, can reach the limiter. Penetrating the ambipolar potential, these electrons complete an electrical circuit by closing on the conducting limiter and vessel walls.

ORNL-DWG 82-2280 FED

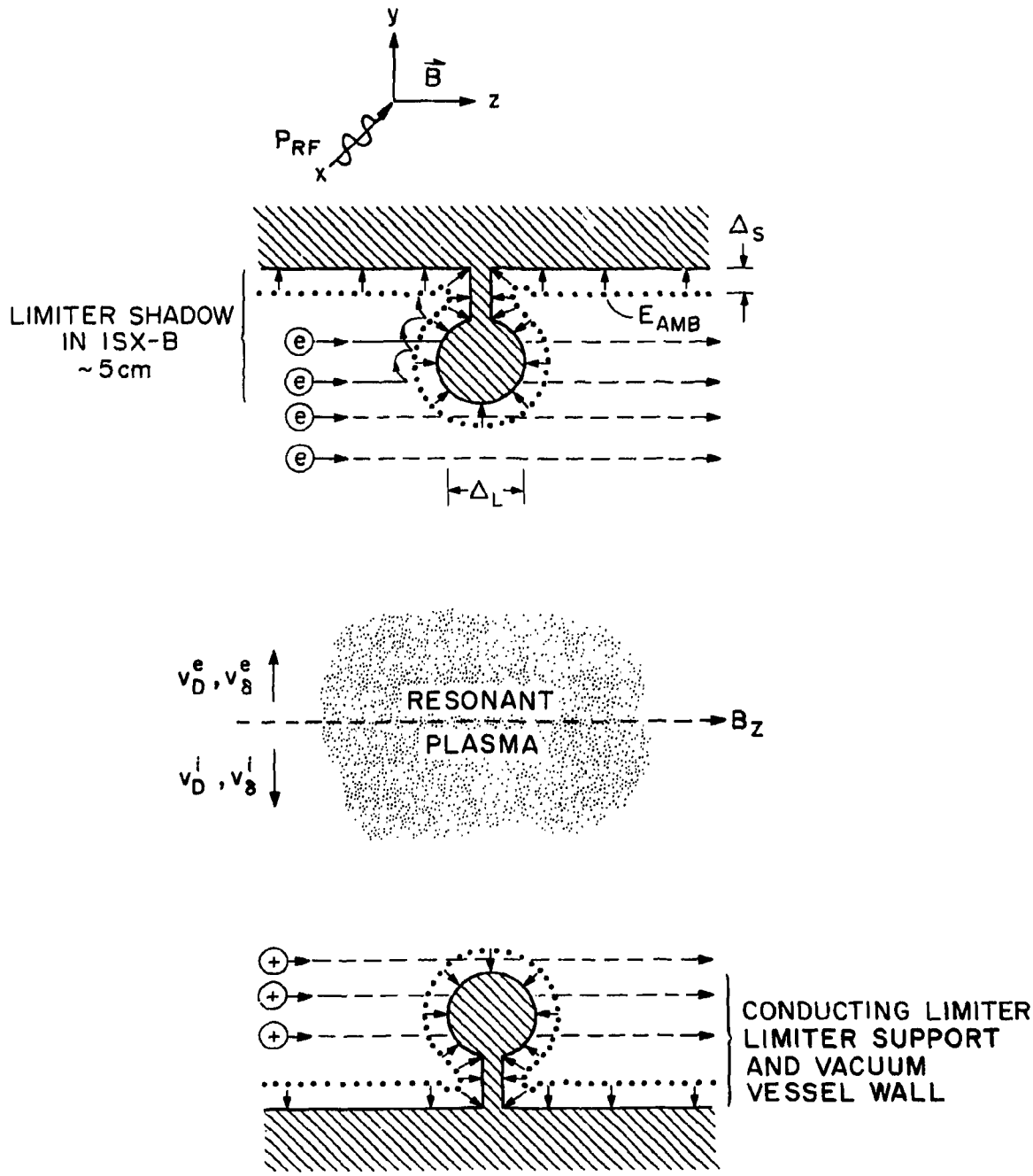

Fig. 3. An illustration of the ISX-B chamber showing particle drift motion and interaction with the horizontal rail limiters and ambipolar sheath potential.

Although the formation of a potential barrier reduces particle and energy loss, the limiters in ISX-B, in some sense, lead to a deterioration in confinement during preheating. By protruding into the plasma they provide an inescapable loss route for all ions and energetic electrons which drift into the limiter shadow. By removing these limiters[13] the motion of both electrons and ions would be affected by $\vec{E}_{AMB} \times \vec{B}$ drift, and confinement could be improved further. Ambipolar transport would then consist of a balance between barrier penetration by tail electrons and collisional diffusion by thermal ions. Stix[14] and Bulyginskii et al.[15] have examined electrostatically assisted toroidal confinement for reactor grade plasmas.

4. PARTICLE AND ENERGY TRANSPORT PRIOR TO CURRENT INITIATION

4.1 PARTICLE BALANCE

Given the effective transfer of wave energy to electrons at the UHR and the existence of an ambipolar potential, a near classical particle and energy transport model is used to estimate the efficiency of electron heating in the absence of plasma current. With electron impact ionization as the primary particle source, the equation for particle balance is given by

$$\frac{dn_e}{dt} = n_e(n_o\langle\sigma v\rangle_{ion} - \tau_e^{-1}) \ , \tag{4.1}$$

where n_o is the neutral particle density and $\langle\sigma v\rangle_{ion}$ is the ionization rate coefficient. The electron loss rate we define,

$$\tau_e^{-1} = \left(\frac{1}{\tau_{De}} + \frac{1}{\tau_{\delta e}}\right) \exp\left\{\frac{|e|\phi_{AMB}}{kT_e}\right\} \ , \tag{4.2}$$

weights the relative importance of curvature and error field drift losses and reflects the fact that only a fraction of the electrons which reach the ambipolar potential can actually penetrate through to the limiter or wall. As we have seen in Eq. (3.3), the value of $e\phi_{AMB}$ depends on the global ion loss rate. In ISX-B, ion confinement is limited to the average drift time by the presence of horizontal rail limiters. Such limiters are not found in FED. Nevertheless, the ion drift time approximation is still used in order to ensure conservative estimates of preheating power for FED (Sect. 6).

4.2 ENERGY BALANCE

The ion temperature is determined by a balance between heating due to collisions with electrons and cooling associated with charge exchange and curvature drift transport. Parallel losses are negligible for the ions except in the case where δB is large (discussed in Sect. 4.4). The electron temperature is determined by rf heating which balances losses resulting from the ionization of neutrals, collisions with ions, Q_{ei}, impurity ionization, p_{ion}, and radiation, p_{rad}, cooling by limiter-emitted secondary electrons, and $\vec{\nabla}B$ and δB drifts. The appropriate balance equations are given by

$$\frac{dE_i}{dt} = \left[\frac{3m_e}{m_i} n_e \frac{k(T_e - T_i)}{\tau_{ei}} - \frac{3}{2} n_e n_o \langle\sigma v\rangle_{cx} k(T_i - T_o) - \frac{3}{2} n_e k T_i \left(\frac{1}{\tau_{Di}} + \frac{1}{\tau_{\delta i}} \right) \right] V_p \tag{4.3}$$

$$\frac{dE_e}{dt} = \left[p_{RF} - n_e n_o \langle\sigma v\rangle_{ion} k W_{ion} - Q_{ei} - (p_{ion} + p_{rad})_{oxygen} - \delta n_e k \frac{(T_e - T_{e2})}{\tau_e} - \frac{\gamma n_e k T_e}{\tau_e} \right] V_p \, . \tag{4.4}$$

Here $\tau_{ei}(m_i/m_e)$ is the electron-ion equilibration time, T_o is the neutral temperature, $\langle\sigma v\rangle_{cx}$ is the charge exchange rate coefficient, p_{RF} is the microwave heating power per unit volume absorbed by electrons over a heating width Δ_H (defined in Sect. 4.3), V_p is the toroidal volume of the vertical heating zone $[= 2\pi R(\sim R_{UH} + \Delta_H/2) \cdot 2b \cdot \Delta_H]$, $E_{e(i)}[= 3/2 \times n_e kT_{e(i)} V_p]$ is the electron (ion) thermal energy content, and kT_{e2} $(\lesssim e\phi_{AMB})$ is the energy of the secondary electron following acceleration through the sheath potential. The parameter W_{ion} is an aggregate energy loss attributed to hydrogen dissociation, ionization, and radiation; it has been assigned a value of 30 eV.[16]

4.3 ELECTRON PREHEATING ASSUMPTIONS

Our analysis of the UHR preheating process has relied on several key assumptions. The first is the existence of a currentless toroidal plasma in which the vertical electric field has been significantly reduced due to the combined presence of an ambipolar electric field and a conducting limiter/vacuum vessel arrangement. In this configuration currents flowing over the conducting walls help to equalize differences in potential,[17] while poloidal $\vec{E}_{AMB} \times \vec{B}$ drift of confined electrons prevents charge buildup and improves confinement. Although not conclusively supporting the above assumption, electron temperature measurements in ISX-B do <u>not</u> confirm a fatal $\vec{E}_v \times \vec{B}$ drift. The following example demonstrates this fact.

In ISX-B [a = 27 cm, b = 50 cm, B (R_o = 93 cm) = 13 kG] electron temperatures of ∿50 eV have been measured near the UHR layer (R_{UH} = 108 cm and $\Delta_H \simeq 4$ cm) at densities of $\sim 3 \times 10^{12}$ cm^{-3}. If the plasma cannot neutralize itself, $\vec{E}_v \times \vec{B}$ drift will cause an outward plasma displacement of Δ in a time given by[18]

$$\tau_{E/B} = \left\{ \frac{\Delta R m_i}{k(T_e + T_i)} \right\}^{1/2} . \tag{4.5}$$

Using the ISX-B parameters along with $\Delta \simeq (R_o + a) - R_{UH} \simeq 12$ cm, $m_i = 1.673 \times 10^{-24}$ g and $T_e/T_i \sim 2$, Eq. (4.5) indicates $\tau_{E/B} \simeq 4.3$ μs. With $3n_e kT_e/2\ \tau_{E/B} \simeq 8.4$ W/cm^3 and $(2\pi R_{UH} \cdot 2b \cdot \Delta_H) \simeq 2.7 \times 10^5$ cm^3, an estimated 2.3 MW of ECRH power is required just to balance plasma transport; this is ∿30 times the available ECRH power used in the ISX-B experiments and therefore suggests significantly better confinement.

Our second assumption is that plasma equilibrium is maintained through the interaction of the toroidal magnetic field and the vertical plasma currents arising from curvature and error field drifts. These currents can form a closed electrical circuit by flowing along magnetic field lines to the conducting limiter and vacuum vessel.[19-21] In the FED the role of a conducting limiter is played by the conducting vacuum vessel itself, which provides the necessary circuit path.

Our final assumption involves our method for estimating Δ_H, the radial extent of the heated electron region. Because of efficient UHR wave absorption and poor, cross-field thermal equilibration, large electron temperature gradients can be produced. Such gradients can lead to possible drift-interchange instabilities and enhanced radial transport, which subsequently broadens the heating region. We estimate the thickness of this broadened layer by assuming that Bohm diffusion "disperses" the heated electrons over a distance Δ_H in a time that is comparable to the electron drift time (the smaller of either τ_{De} or $\tau_{\delta e}$). Setting τ_{BOHM} equal to τ_{De} and $\tau_{\delta e}$ leads to the expression

$$\frac{\Delta_H^2\ B}{6.25 \times 10^6\ T_e} \simeq \begin{cases} bRB/(2 \times 10^8\ T_e) & ;\ \tau_{De} << \tau_{\delta e} \quad (4.6) \\ (bB/\delta B)/(3.3 \times 10^7\ T_e^{1/2}) & ;\ \tau_{\delta e} << \tau_{De} \quad (4.7) \end{cases},$$

from which one obtains

$$\Delta_H \simeq \begin{cases} 0.177(bR)^{1/2} & ;\ \tau_{De} << \tau_{\delta e} \quad (4.8) \\ 0.433(b/\delta B)^{1/2}\ T_e^{1/4} & ;\ \tau_{\delta e} << \tau_{De} \quad (4.9) \end{cases}.$$

Here, b is the vertical half-height of the vacuum chamber at $R = R_{UH}$. As indicated above the value of Δ_H depends primarily on size and on the level of magnetic field error present in the device.

4.4 TRANSPORT REGIMES OF INTEREST

The magnitude of the ambipolar potential that arises during preheating will depend sensitively on whether transport is dominated by curvature drift ($\tau_\delta >> \tau_D$) or parallel drift loss ($\tau_\delta << \tau_D$). Magnetic perturbations of the toroidal field structure can cause field lines to spiral out of the chamber where they may intercept the limiter or vessel walls. Error fields of only a few gauss can significantly impact plasma confinement in both the bulk and UHR regions. Equations (3.1) and (3.2) indicate that if δB satisfies

$$\delta B \gtrsim 1.98 \times 10^{14} \frac{\sqrt{m_j T_j}}{R} \quad ; \; j = e,i \; , \tag{4.10}$$

losses due to error fields cannot be neglected. For a hydrogen plasma, Eq. (4.10) simplifies to

$$\delta B \gtrsim \begin{Bmatrix} 6\ T_e^{1/2}/R \\ 256\ T_i^{1/2}/R \end{Bmatrix} \quad \text{for} \quad \begin{Bmatrix} V_{\delta e} \gtrsim V_{De} \\ V_{\delta i} \gtrsim V_{Di} \end{Bmatrix} . \qquad \begin{matrix} (4.11) \\ (4.12) \end{matrix}$$

Because $V_{\delta e}/V_{\delta i} > \sqrt{m_i/m_e}$, large levels of magnetic field error are required to affect ion transport.

Various transport regimes may exist in the ISX-B tokamak (Fig. 2b) depending on the magnitude of the error fields present in the device. In this study we assume that the major component of δB is in the vertical direction (i.e., parallel to the major axis of the torus) and that parallel losses add to those associated with the toroidal drift. Potential sources of vertical error fields are the geomagnetic fields and the residual magnetization of the ISX-B iron core. Because ISX-B is not

shielded against such vertical error fields, we expect ISX-B to operate in regime II. For R_o = 93 cm, $B(R_o)$ = 13 kG, b = 50 cm, $R_{UH} \simeq$ 108 cm, and $T_e \simeq$ 50 eV, Eqs. (3.1) and (3.2) indicate that $\tau_{De} \simeq$ 6 ms and $\tau_{\delta e} \simeq$ (2.75/δB) ms. In larger, D-shaped, reactor-grade plasmas such as FED [R_o = 480 cm, $B(R_o)$ = 36.2 kG, a = 130 cm, σ = 1.6, and $b(R_{UH}$ = 590 cm) $\simeq$ 100 cm], $\tau_{De} \simeq$ 87 ms and $\tau_{\delta e} \simeq$ (9/δB) ms for electrons preheated to $\sim$100 eV. It is apparent that increases in size and magnetic field strength can lead to significant improvements in confinement provided effective error field control can be realized. For example, requiring that $\tau_{De} = \tau_{\delta e}$ would dictate designing a large and complex coil system to a tolerance level of $\delta B/B \lesssim 3 \times 10^{-6}$. Such levels may be difficult to achieve in FED-size devices. Error field levels as low as $\delta B/B \sim 0.5 \times 10^{-4}$ have been achieved in the closed field line EBT device[22] using a combination of control techniques. These techniques include electron beam alignment of the toroidal mirror coil geometry and the use of error field compensation coils during operation.

5. COMPARISON WITH ISX-B EXPERIMENTAL RESULTS

During recent preheating experiments on ISX-B (Fig. 2a), a 35-GHz gyrotron was used to inject $\sim$70-80 kW of microwave power into the plasma for up to 15 ms.[8,9] The ECRH power, which contained equal mixtures of ordinary and extraordinary mode waves, was launched from the high field side at an angle of 45° to the major radius.

A variety of diagnostic techniques were used to study the characteristics of the preheated plasma. The following list summarizes the experimental findings of Ref. 8:

(1) Plasma formation is initiated in a narrow, vertical layer located at the cyclotron resonance [R_{EC} = 97 cm for $B(R_o$ = 93 cm) = 13 kG].

(2) Within a fraction of a millisecond, some of the plasma reaches the top of the ISX-B chamber.

(3) As the density builds, the vertical layer moves outward to a location of lower magnetic field corresponding to the upper hybrid resonance (at $n_e = 3 \times 10^{12}$ cm^{-3}, $R_{UH} \approx 108$ cm). This spatial transition is observed in both time-resolved density profiles and high-speed movies of the preheating process.

(4) After ∿5 ms of rf heating, a flat density profile is measured with an average density of $n_e \simeq 3 \times 10^{12}$ cm^{-3}. Measurements are made using on-axis vertical and horizontal microwave interferometers.

(5) The electron temperature in the bulk plasma is estimated to be 11-13 eV based on spectroscopic measurements of oxygen impurity. A lower estimate of 8-10 eV is obtained using a particle energy analyzer (PEA) which is inserted into the center of the plasma.

(6) An electron temperature of ∿50 eV is measured (using the PEA) over a 4-cm-thick region centered at $R_{UH} = 108$ cm.

(7) The preheated plasma appears macroscopically stable 5 ms after the microwave power is turned on. It remains quiescent during the remainder of the 15-ms rf pulse.

(8) Once the rf power is terminated, the density decays to half its value in about 10 ms. This half-life indicates a bulk plasma temperature of ∿20 eV if the decay is due to curvature drift.

(9) Spectroscopic and radiometric data prove that radiation cooling is <u>not</u> a dominant loss mechanism in the preheated plasma. Of the 5 kW of radiated power measured, only about 20% is from impurities and the remaining 80% is from hydrogen.

This last experimental observation is most interesting because it contradicts the theoretical analysis of Ref. 8, which suggests that oxygen radiation is responsible for most (∿75 kW) of the injected microwave power.

5.1 THEORY VS EXPERIMENT

In an effort to explain the preheating experiments, we have reanalyzed the ISX-B results using the theoretical model for UHR heating presented in the previous sections. With $T_e \simeq 10$ eV, $n_e \simeq 3 \times 10^{12}$ cm^{-3}, and $f_{RF} = 35$ GHz, Eq. (2.1) indicates that wave absorption will occur primarily at the UHR layer. According to Eq. (2.3), this layer is located at $R_{UH} \simeq 108$ cm for $\alpha \simeq 0.2$ and $R_{EC} = 97$ cm. The significant electron heating expected at R_{UH} is also substantiated by the 50 eV electron temperatures measured at R = 106 and 110 cm. We interpret the hot plasma measured outboard of the UHR layer as evidence supporting a broadening of the heated electron region. Because T_e measurements were not made beyond 110 cm, the actual extent of the heating region is unknown. However, by assuming that error field losses dominate electron transport, we can estimate the width of the heated electron region using Eq. (4.9). Our calculations indicate that Δ_H can vary from ∿8-4 cm for $T_e = 50$ eV and $\delta B = 1$-4 G.

Because of the apparent leveling off of the plasma density and temperature after several milliseconds of preheating,[8] the equations for particle [Eq. (4.1)] and energy balance [Eqs. (4.3) and (4.4)] have been solved as steady-state equations. Before one can estimate the ECRH power required to balance the various electron energy losses, it is necessary to first determine the confining ambipolar potential. Our procedure for estimating ϕ_{AMB} is to first eliminate the neutral density (n_o) from the ion energy balance using Eq. (4.1). With the plasma density held fixed at $n_e \simeq 3 \times 10^{12}$ cm^{-3}, we then solve Eq. (4.3) for ϕ_{AMB} as a function of T_i. Estimates of ϕ_{AMB} are made in both the bulk and UHR regions using a range of electron temperatures and error field values believed to be characteristic of that region. However, only those self-consistent sets of parameters (corresponding to a single value of ϕ_{AMB}) that satisfy Eq. (3.3) constitute a bonafide "zero net current" solution determining the global ambipolar potential. Once ϕ_{AMB} is known, the neutral density and ECRH power requirements for each region can be obtained using Eqs. (4.1) and (4.4).

Steady-state solutions, representing a number of ambipolar equilibria, have been generated for comparison with experiment. The results are summarized in Tables 1 and 2. Using the plasma parameters measured in ISX-B, Table 1 shows the required ECRH power as a function of error field value and secondary electron emission.

5.1.1 Effect of Error Fields

As Table 1 indicates, increasing values of δB lead to a decrease in electron confinement and a rise in the ambipolar potential. Error fields have little effect on ion transport which remains dominated by curvature drift losses. In the absence of secondary electron emission, the ambipolar potential is very effective in confining the bulk electrons. Such increased confinement leads to low values of neutral density in the bulk plasma. This fact, together with the lengthy confinement time for ions ($\sim$30 ms), results in a negligible power loss from the bulk plasma.

In the UHR region, however, $e\phi_{AMB}/kT_{eH}$ is of order unity, and a greater percentage of heated electrons escape to the limiter. Transport losses from this region account for $\sim$60 to 70% of the calculated ECRH power. Collisional cooling of electrons on ions and neutral hydrogen ionization (listed in order of their importance) account for the remaining power.

5.1.2 Secondary Electron Emission

Those heated electrons which succeed in hitting the stainless steel limiters in ISX-B can possess sufficient energy to cause secondary electron emission. Data showing the secondary electron yield (δ) for stainless steel as a function of primary electron energy has been given by Hall.[23] This data has been extrapolated to a lower range of electron temperatures (10 eV $\leq T_e \leq$ 100 eV) in order to examine the effects of secondary emission on particle and energy transport in ISX-B. As Table 1 shows, secondary electrons can cause a substantial reduction in the sheath potential (by as much as 60 to 70%). However, at $T_{ec} \simeq$ 10 eV and $T_{eH} \simeq$ 50 eV the resulting deterioration in confinement does not

Table 1. Estimates of key plasma parameters and required ECRH power in ISX-B for $n_e = 3 \times 10^{12}$ cm^{-3} and several values of δB without and with secondary electron emission

$\delta_c = 0.0$, $\delta_H = 0.0$	$\delta B = 1$ G		$= 2$ G		$= 4$ G	
T_e (eV)	10	50	10	50	10	50
T_i (eV)	9.87	25.9	9.87	23.2	9.85	19.5
τ_{De} (ms)	30.2	6.05	30.2	6.05	30.2	6.05
$\tau_{\delta e}$ (ms)	6.15	2.75	3.08	1.38	1.54	0.69
τ_{Di} (ms)	30.6	11.7	30.6	13.0	30.7	15.5
$\tau_{\delta i}$ (ms)	265	164	133	86.6	66.4	47.2
ϕ_{AMB} (V)	-39.0		-47.4		-54.3	
n_o (10^{10}cm^{-3})	0.068	0.89	0.054	1.27	0.051	2.01
Δ_H (cm)	-	8.1	-	5.8	-	4.1
V_H (10^6cm^3) [a]	-	0.56	-	0.40	-	0.28
V_C (10^6cm^3) [b]	2.59	-	2.75	-	2.87	-
P_{ECRH} (kW)	1.3	12.9	1.3	12.8	1.5	13.8
$\delta_c \simeq 0.1$, $\delta_H \simeq 0.5$	$\delta B = 1$ G		$= 2$ G		$= 4$ G	
T_e (eV)	10	50	10	50	10	50
T_i (eV)	9.76	23.6	9.76	20.5	9.74	16.9
τ_{De} (ms)	30.2	6.05	30.2	6.05	30.2	6.05
$\tau_{\delta e}$ (ms)	6.15	2.75	3.08	1.38	1.54	0.69
τ_{Di} (ms)	31.0	12.8	31.0	14.7	31.0	17.9
$\tau_{\delta i}$ (ms)	267	172	133	91.9	66.8	50.7
ϕ_{AMB} (V)	-22.9		-30.1		-36.2	
n_o (10^{10}cm^{-3})	0.34	1.23	0.30	1.80	0.31	2.89
Δ_H (cm)	-	8.1	-	5.8	-	4.1
V_H (10^6cm^3)	-	0.56	-	0.40	-	0.28
V_c (10^6cm^3)	2.59	-	2.75	-	2.87	-
P_{ECRH} (kW)	3.2	16.3	3.4	15.9	3.9	16.8

[a] $V_H = 2\pi R_{UH} \cdot 2b \cdot \Delta_H$.
[b] $V_c = V_p - V_H$, where $V_p = 2\pi R_o \cdot 2b \cdot 2a = 3.15 \times 10^6$ cm^3.

Table 2. Estimates of the same key parameters and ECRH power for several different cold/hot electron temperatures

$\delta_c \simeq 0.1$, $\delta_H \simeq 0.7$	$\delta B = 1$ G		$= 2$ G		$= 4$ G	
T_e (eV)	20	70	20	70	20	70
T_i (eV)	17.9	23.3	17.9	20.1	17.7	16.5
τ_{De} (ms)	15.1	4.32	15.1	4.32	15.1	4.32
$\tau_{\delta e}$ (ms)	4.35	2.33	2.18	1.16	1.09	0.58
τ_{Di} (ms)	16.9	13.0	16.9	15.0	17.1	18.4
$\tau_{\delta i}$ (ms)	197	173	98.5	92.9	49.5	51.4
ϕ_{AMB} (V)	-32.0		-43.5		-54.4	
n_o (10^{10}cm^{-3})	0.39	1.41	0.39	1.97	0.42	3.01
Δ_H (cm)	-	8.9	-	6.3	-	4.4
V_H (10^6cm^3)	-	0.62	-	0.43	-	0.30
V_c (10^6cm^3)	2.53	-	2.72	-	2.85	-
P_{ECRH} (kW)	11.0	25.9	13.3	23.8	16.0	23.6
$\delta_c \simeq 0.1$, $\delta_H \simeq 0.8$	$\delta B = 1$ G		$= 2$ G		$= 4$ G	
T_e (eV)	20	100	20	100	20	100
T_i (eV)	17.8	18.4	17.8	15.0	17.6	11.3
τ_{De} (ms)	15.1	3.02	15.1	3.02	15.1	3.02
$\tau_{\delta e}$ (ms)	4.35	1.95	2.18	0.97	1.09	0.49
τ_{Di} (ms)	17.0	16.4	17.0	20.2	17.2	26.8
$\tau_{\delta i}$ (ms)	198	194	98.8	108	49.7	62.1
ϕ_{AMB} (V)	-33.8		-45.4		-56.4	
n_o (10^{10}cm^{-3})	0.36	1.92	0.35	2.75	0.38	4.32
Δ_H (cm)	-	9.7	-	6.8	-	4.8
V_H (10^6cm^3)	-	0.68	-	0.47	-	0.33
V_c (10^6cm^3)	2.47	-	2.68	-	2.82	-
P_{ECRH} (kW)	10.4	52.5	12.8	49.3	15.3	51.2

translate into a large increase in hot plasma transport because ∿50% of the sheath sustaining energy is automatically returned to the plasma by the secondary electrons. The additional power requirements in the UHR region are due mainly to increased neutral ionization losses and collisional electron cooling on colder, secondary electrons. These secondary electrons equilibrate rapidly (<5 μs) with the heated electrons and account for roughly 1.5 to 2.0 kW of additional ECRH power. In the bulk plasma, the higher ECRH power needs are due to increased neutral ionization and transport. Potential heating of the bulk electrons by the more energetic secondary electrons has been neglected in the bulk plasma power estimates.

5.1.3 Evidence of Higher Electron Temperatures

Even with secondary electron emission included in our theoretical estimates, we can, at best, account for only 25% of the injected rf power using the electron temperatures reported in Ref. 8. The lack of agreement between theory and experiment at these temperatures has prompted us to consider a higher range of values for both the bulk and UHR region. Indications of higher electron temperatures ($T_{ec} \simeq 20$ eV and $T_{eH} \lesssim 100$ eV) can, in fact, be inferred from several of the experimental findings (5, 6, and 8) mentioned at the beginning of this section. The sensitivity of the ECRH preheating power to different cold/hot electron temperature combinations is shown in Table 2. Here, one notices that there is a significant increase in the ECRH power requirements. At $T_{eH} = 70$ eV, $P_{ECRH} \lesssim 40$ kW, and at $T_{eH} = 100$ eV, $P_{ECRH} \lesssim 66$ kW. Enhanced transport accounts for most of the observed increase in the UHR region (∿15 kW at $T_{eH} = 70$ eV and ∿35 kW at $T_{eH} = 100$ eV). Because the percentage of secondary emission increases with electron temperature, the ambipolar potential remains roughly constant (for a given error field value), despite the rising temperatures. Under these conditions a larger number of hot electrons will be lost from the UHR layer and, in their place, cold secondary electrons will be accelerated back in. This exchange of cold-for-hot electrons satisfies the ambipolarity constraint, but it also leads to a sizeable electron energy loss. The equilibration

of the secondary electrons with their hot counterparts causes a further energy drain amounting to $\sim$10 kW (for $T_{eH} \simeq 100$ eV). In the bulk plasma, the nonresonant absorption of rf power balances losses due to electron-ion collisions ($\sim$5 to 7 kW), transport ($\sim$3 to 7 kW), and neutral ionization ($\sim$2 to 3 kW). Because the rf power requirements in the heated plasma exceed the 40 kW of extraordinary mode radiation, some absorption of the ordinary mode ($\sim$10 kW) is also indicated. Despite the fact that the preheated plasma is optically thin to the O-mode at the plasma parameters being discussed, effective absorption should still be possible because of multiple reflections and the potential for repolarization at the vacuum vessel walls.

Before concluding this section, a comparison between our theoretical results (at $T_{ec} = 20$ eV/$T_{eH} = 100$ eV) and the ISX-B experimental observations is in order. According to our theoretical model, the formation of an ambipolar potential is a direct consequence of ECRH. The radial electric field ($\vec{E}_{AMB}$), which forms between the neutral plasma and the vacuum vessel, enables the plasma to neutralize itself via poloidal $\vec{E}_{AMB} \times \vec{B}$ drift. The ambipolar equilibrium which results may explain the quiescent nature of the preheated plasma and the absence of large scale $\vec{E}_V \times \vec{B}$ drift. This ambipolar potential improves bulk electron confinement and allows significant electron-ion temperature equilibration to occur. Using $\Sigma\dot{N}_i = n_i V_p/\tau_{pi}$ to define a global ion confinement time, we find that $\tau_{pi} \simeq 16$-13 ms for $\delta B = 1$-4 G. These values compare favorably with the experimental estimate of $\sim$15 ms. It also suggests that plasma decay in ISX-B is controlled mainly by ion transport. Because oxygen radiation is negligible in the ISX-B experiment, it has not been included in our power balance calculations. However, we have estimated that $\sim$8 kW (total for both regions) is required for neutral hydrogen ionization. By assuming that roughly half of the 30 eV needed for ionization is associated with line radiation, we find that the resulting 4 kW is consistent with spectroscopy and radiometry measurements for hydrogen. Finally, our estimates for Δ_H ($\sim$5-10 cm) and P_{ECRH} ($\lesssim$66 kW) appear to be in reasonably good agreement with the experimental data ($\Delta_H \gtrsim 4$ cm and $P_{ECRH} \simeq 70$-80 kW). In order to be fair in our comparison we should

point out that our theoretical results are sensitive to the values of δ selected. Reference 23 indicates that $\delta \lesssim 1.0$ at $T_e \simeq 100$ eV. We have, however, specified that δ is not to exceed ~ 0.8, a value which corresponds to saturated emission[12] in a hydrogen plasma. As a final consideration, we have assumed that unipolar arcing[24] is unimportant. Although estimates of the triggering potential for arcing range from a few tens[24] to several hundred eV,[25] the signature of arcing (significant impurity production) has not been observed in the experiments.

The results just presented provide a plausible interpretation of the available ISX-B data. However, in order to rigorously test the UHR heating model, the experimental data base should be expanded to include measurements of all key parameters (T_e, T_i, n_e, n_o, δB, and Δ_H). For example, by monitoring the particle current to the ISX-B limiters and utilizing infrared camera measurements, valuable data concerning particle and energy transport during preheating could be obtained.

6. APPLICATION TO THE FED TOKAMAK

Encouraged by the reasonably good agreement, to date, between theory and experiment, the UHR heating model has been applied to FED to assess the ECRH power requirement and its sensitivity to uncertainties in temperature, error field, δB, ambipolar potential, ϕ_{AMB}, and impurity content. Our results, summarized in Table 3, are based on several assumptions. These include (1) total absorption of the EO-mode wave energy at the UHR layer with very little nonresonant heating of the inner bulk plasma and (2) a dynamic density startup. In the later, it is assumed that preheating commences from a prefill pressure of $\sim 10^{-5}$ torr. As electrons heat and the ionization rate becomes substantial, the plasma density increases to 10^{19} m^{-3} in the UHR region as neutrals are pumped from the remaining chamber volume. Inherent in this second assumption is a controlled neutral gas feed capability and the absence of significant sources or sinks on the chamber wall.

Table 3. Dependence of ECRH preheating power requirment P_{ECRH} on poloidal error field δB, T_e, the ambipolar potential ϕ_{amb}, and the impurity content in FED

Parameters	Poloidal error field δB = 2G			Poloidal error field δB = 0		
T_e(eV)	20	100	200	20	100	200
T_i(eV)	∿20	92	144	∿20	94	154
$\tau_{\delta e}$(ms)	10	4.4	3.1	-	-	-
τ_{De}(ms)	430	87	43	430	87	43
Δ_H(cm)	6.5	10	12	42	42	42
V_H(m^3)	4.8	7.5	8.7	31	31	31
Φ_{amb}/T_e	-3.1→0	-2.7→0	-2.7→0	∿0	∿0	∿0
P_{ECRH}(MW)						
(1% oxygen)	0.44→0.46	0.15→0.50	0.48→1.65	2.8	0.31	0.98
(3% oxygen)	1.30→1.32	0.16→0.51	0.50→1.68	8.4	0.34	1.07

Examining Table 3, it is apparent that increasing levels of oxygen contaminate can have a strong impact on the rf power requirement before the electron temperature is raised beyond the radiation barrier (occurring at $T_e \simeq 20$ eV). It is also noted that these results may be somewhat optimistic because the radiation model used[26] assumes coronal equilibrium. Once this critical barrier temperature is surpassed, the required ECRH power drops sharply and is determined primarily by error field transport and collisional cooling of electrons on ions. The ions in turn lose energy mainly through charge exchange with cold neutrals ($T_o \lesssim 0$ eV is assumed).

Table 3 also illustrates that the presence of a low error field (2 G) is sufficient to dominant electron transport. Error field levels higher than those shown can significantly reduce the confinement time and compete with cross-field Bohm diffusion to bring about a large decrease in the heated volume. This results in only a modest decrease in loop voltage during the subsequent current start-up phase. In contrast to the small ISX-B tokamak ($\tau_{\delta e} \lesssim \tau_{De}$), rapid electron loss in FED ($\tau_{\delta e} << \tau_{De}$) results in large ambipolar potentials ($e\phi_{AMB}/kT_e \sim 3$), which can exceed the triggering potential for unipolar arcing. Secondary electron emission from the walls can also lead to a deterioration of the ambipolar potential and an increase in P_{ECRH}. We have exaggerated the actual value of this increase (a factor of 2 to 3) by assuming $\phi_{AMB} \to 0$. In reality, for electron temperatures $\gtrsim 100$ eV, secondary emission will saturate at $\delta \sim 0.8$, causing the sheath potential to fall to a minimum value of order $e\phi_{AMB}/kT_e \sim 1$. With no error fields present, there is an improvement in confinement leading to $T_e \simeq T_i$, $\phi_{AMB} \simeq 0$ and a factor of ~ 4 increase in $\Delta_H[\propto (bR)^{1/2}]$. Because the volume of the heated plasma has increased by a factor of ~ 6, oxygen losses can become quite prohibitive at $T_e \simeq 20$ eV. Finally for $\phi_{AMB} \sim 0$, a continuous conducting limiter or vacuum vessel becomes essential to prevent the buildup of a large vertical electric field.

These results suggest the following approach to electron heating prior to current initiation. In the presence of a low poloidal error field (~ 2 G), ECRH power up to 2 MW is injected to burn through the impurity radiation barrier in the UHR region, achieving $T_e \lesssim 100$ eV.

The initial heating volume, estimated to be about 5 m^3 would be produced in a time scale <50 ms. The error field would then be eliminated near the heating zone (e.g., via field cancelling coils), thereby allowing the heated volume to increase to about 30 m^3. The ECRH power can then be reduced to about 1 MW, sustaining an electron temperature of $\sim$100 eV at a density of about 10^{19} m^{-3}.

7. CURRENT INITIATION AND RAMP-UP

The UHR electron heating just discussed leads naturally to the formation of a small radius current channel centered at the UHR layer. It is predominantly in this region of high T_e that the plasma current will be induced once the toroidal loop voltage is applied. The ensuing rotational transform is expected to "smear out" the energy content of the axisymmetric vertical absorption layer as flux surfaces begin to form. This will lead to substantial electron cooling over most of the plasma cross section except for a small inner region of radius $a_o \gtrsim \Delta_H$ localized at R_{UH}.

In FED such a small radius plasma is formed by applying a relatively low voltage using programmed current ramps in the ohmic heating and blip coils. This allows the plasma current to increase to a level consistent with a specified edge safety factor, q_I.* During this phase, the small radius plasma (a_o = 0.2 m) maintains its radial location (R = 5.9 m) against fixed start-up limiters located at the outboard midplane; the time duration is $\sim$0.2 s. Over the major portion of this time scale, the current ramp time satisfies the physics constraint $\tau_I (= I_p/\dot{I}_p) > \tau_s$ (the plasma skin time). This prevents the formation of skin currents and minimizes the potential hazards of plasma disruption.[27] For comparison, calculations have also been done for a larger start-up radius plasma (a_o = 0.4 m). Because $\tau_s (= \mu_o a^2/\eta_{\parallel})$ is proportional to $a^2 T_e^{3/2}/Z_{eff}$, the a_o = 0.4 m case will require roughly a factor of 4 increase in the

---

*For a circular plasma [appropriately modified for elongation (σ) effects], the "safety factor" is defined as

$$q_I \equiv \frac{2\pi a^2 B(R)}{\mu_o I_p R} \left(\frac{1 + \sigma^2}{2}\right) .$$

current ramp period for a comparable level of electron preheating. About 1 MW of extraordinary mode, ECRH (at 87 GHz for a_o = 0.2 m and 90 GHz for a_o = 0.4 m), is maintained to ensure a proper electron temperature during current initiation.

Having achieved the desired value of q_I at the plasma/limiter edge, the major radius $R_{initial}$ (= R_{UH}) is shifted inward and a new layer of plasma is added to the warm core through ionization of a regulated gas feed (Fig. 4). This major radius compression permits minor radius expansion (to a = 1.3 m and σ = 1.6) and the simultaneous increase in plasma current (to I_p = 4.8 MA), while maintaining a constant q_I. The R-compression is achieved through appropriate feedback control of the vertical magnetic field [sensing on $I_p(t)$]. The instantaneous major radius of the expanding plasma is given by

$$R(t) = \frac{R_{LIM}}{[1 + \varepsilon(t)]} \tag{7.1}$$

where

$$\varepsilon(t) \equiv \frac{a(t)}{R(t)} = \left\{ \left[\frac{\mu_o q_I I_p(t)}{2\pi B(R_o) \cdot R_o} \right] \left[\frac{2}{1 + \sigma^2(t)} \right] \right\}^{1/2} , \tag{7.2}$$

and

$$R_{LIM} = 6.1 \text{ m} = R(t) + a(t) \tag{7.3}$$

is the major radius location of the outboard start-up limiters. The initial minor radius is specified to be $a(t = 0) = a_o$ = 0.2 m or 0.4 m. Using Eqs. (7.3) and (7.1), the corresponding instantaneous plasma radius is given by

$$a(t) = R_{LIM} \left\{ \frac{\varepsilon(t)}{1 + \varepsilon(t)} \right\} . \tag{7.4}$$

ORNL-DWG 81-17283RFED

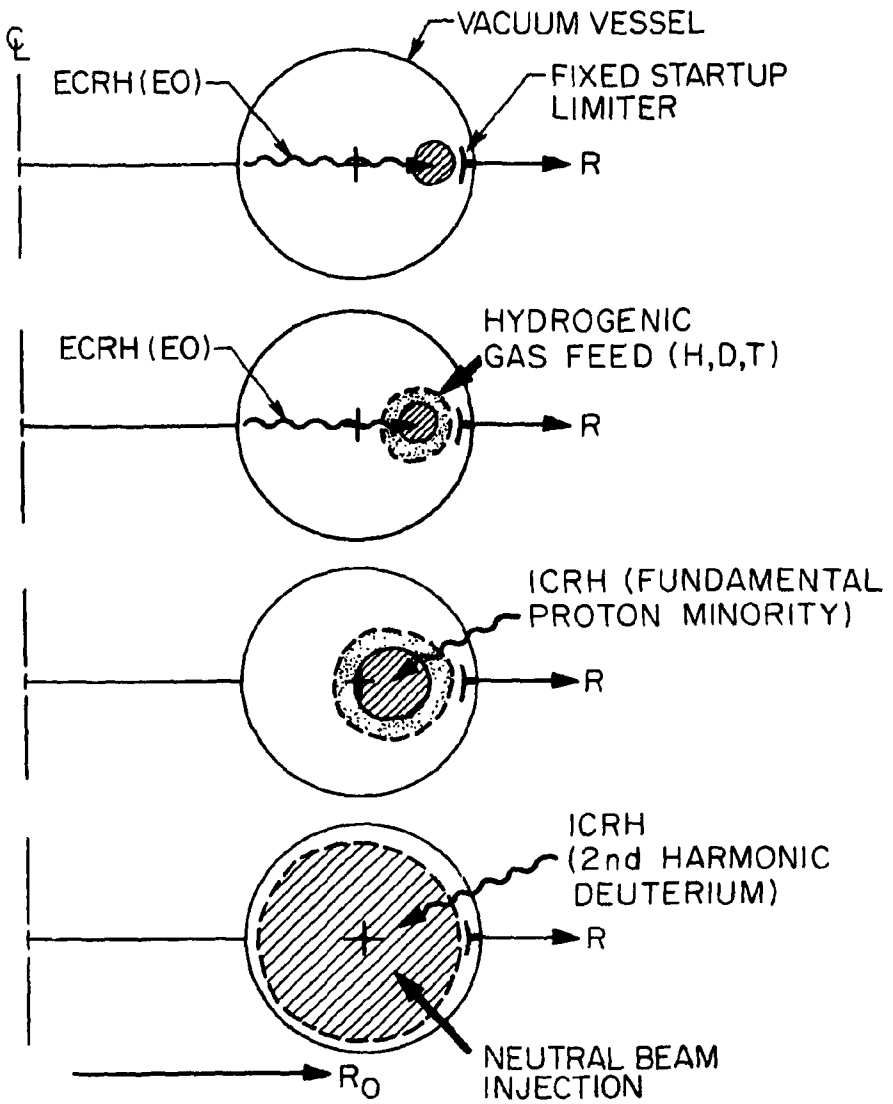

Fig. 4. A constant q_I minor radius expansion with major radius compression and rf assist.

With the onset of major radius compression, additional rf power (∿4 MW) is applied to the plasma. Because of the modest plasma parameters ($n_e \gtrsim 10^{19}$ m^{-3}, $T_e \simeq 0.1$-0.2 keV, and $I_p \simeq 0.04$-0.18 MA) that exist at this time, wave absorption and heating are most efficiently achieved using EO-mode, ECRH. As the plasma current and density are ramped up, cyclotron damping will increase[5] shifting the location of wave absorption back to the cyclotron layer ($R_{EC} \simeq 5.6$ m for $f_{RF} = 87$ GHz and $\simeq 5.4$ m for $f_{RF} = 90$ GHz). Because of this effect, a single rf frequency should provide adequate plasma heating during the compression from R_{UH} (= 5.9 m for $a_o = 0.2$ m and 5.7 m for $a_o = 0.4$ m) to R_{EC}. To continue with ECRH beyond this point requires going to higher frequencies (∿100 GHz for $R_{EC} = R_o = 4.8$ m) for better on-axis heating. Although a 100-GHz capability is being provided for FED, ion cyclotron resonance heating (ICRH) of a deliberately introduced proton minority[28] is a convenient option with which to continue heating. The required frequency range is approximately 47-54 MHz and low field side injection is possible. Furthermore, minority heating would be initiated at a point where the plasma size is comparable to PLT and the plasma currents are of order ∿0.5 MA, ensuring adequate confinement of the energetic protons.

Because of the substantial starting densities ($n_e \simeq n_i \simeq 10^{19}$ m^{-3}), good Coulomb coupling between the electrons and ions should ensure approximate equality of their respective temperatures. The purpose of the ECRH/ICRH power is to supplement the ohmic heating and eliminate the need for a fast current rise. By producing and maintaining a reasonably high plasma conductivity and extending the startup times (∿5-6 s), the initial voltage demands can be significantly reduced (to ∿25 V), compared to the purely inductive current startup (≳100 V). The additional ECRH/ICRH power can also reduce the impact of impurities on resistive volt-second consumption during the current ramp.

7.1 EXPANDING PLASMA OPTIONS

A constant q_I plasma expansion involving R-compression is the proposed scenario for current start-up in the FED.[1] The advantages to be gained by utilizing this expanding radius technique are the avoidance of

skin current effects[29] and an ability to tailor the current profile as the plasma radius is increased.[30] This startup approach is also one that can be tried on the Tokamak Fusion Test Reactor (TFTR)[31] over the next several years. Given the feasibility of high field injection on TFTR, a 60-GHz demonstration test of this expanding radius option (from $a_o \simeq 0.2$ m and $n_e \simeq 10^{19}$ m^{-3}) is possible under low toroidal field operation, $B(R_o = 2.65 \text{ m}) = 2.5$ T. A disadvantage, however, of the R-compression scenario is that the plasma axis is continually forced into regions of higher magnetic field during the expansion. This shifts the location of cyclotron resonance and necessitates multiple frequency operation with its added technological complexity.

An alternative to the compressed major radius approach involves a constant q_I expansion from a fixed major radius (Fig. 5). Once the desired q_I value is achieved, the minor radius and plasma current are simultaneously increased to their full-size ohmic values. The actual radius expansion is performed in a controlled manner using a retractable limiter. The withdrawal rate is synchronized with the rising plasma current and satisfies the relationship $a(t) = R_o\varepsilon(t)$. This leads to the formation of uniform current densities while maintaining a constant q_I. Although the initial ECRH frequency required for preheating is higher, this approach offers the advantage that a single frequency can be used for on-axis heating during the entire plasma expansion. This is particularly true for the higher field tokamak designs like ETF/INTOR,[32,33] where the UHR and ECR layers are in close proximity to each other.

In terms of technological requirements, a moveable limiter is needed to define the plasma size during the expansion phase. Such retractable limiters are planned for use on the large Japanese tokamak, JT-60.[34] The information gained from this experiment and TFTR should help to delineate the potential advantages (or disadvantages) between these two expanding radius options.

ORNL-DWG 81-17284RFED

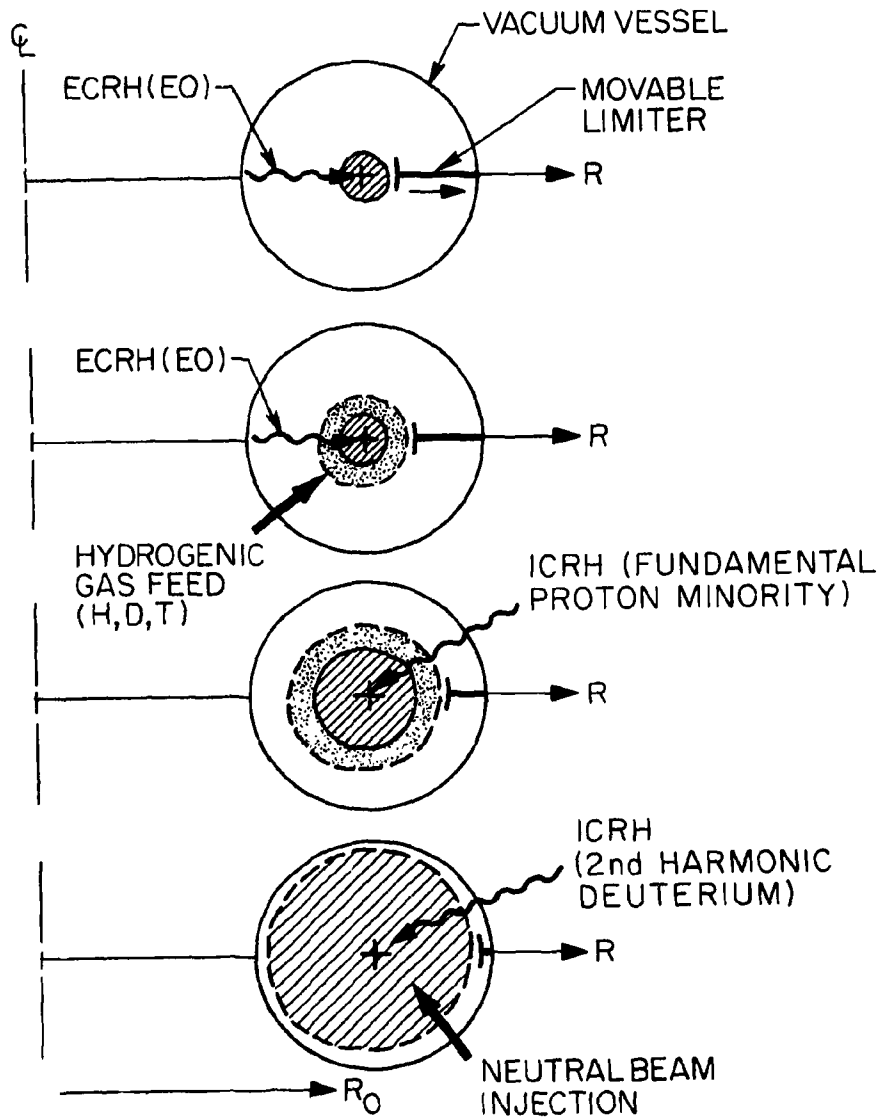

Fig. 5. A constant q_I minor radius expansion with fixed major radius and rf assist.

8. START-UP VOLTAGE AND VOLT-SECOND REQUIREMENTS

8.1 ELECTRON TEMPERATURE ESTIMATES DURING CURRENT STARTUP

In order to assess the voltage and flux requirements during startup, the time history of the electron temperature is needed. A reasonable estimate of $T_e(t)$ can be obtained using the following simple, plasma particle and energy balance equations (mks units with T in keV):

$$\frac{dn_e}{dt} = n_e n_o \langle\sigma v\rangle_{ion} - \frac{n_e}{\tau_p} , \tag{8.1}$$

$$\frac{dn_o}{dt} = -n_e n_o \langle\sigma v\rangle_{ion} + \frac{n_e}{\tau_p} f_R + S_{EXT} , \tag{8.2}$$

$$\frac{dW_p}{dt} = P_{oh} + P_{rf} - P_{ion} - P_{cx} - P_{rad} - \frac{W_p}{\tau_E} , \tag{8.3}$$

where

$\tau_E = \tau_{Ei} = \tau_{Ee} (= 5 \times 10^{-21}\ n_e a^2_{eff} [a^2_{eff} = a^2\sigma])$ is the energy confinement time,

$\tau_p (= 3\ \tau_E)$ is the particle confinement time,

$W_p [= 3/2\ n_e k (T_e + T_i) V_p]$ is the plasma thermal energy,

$V_p (= 2\pi^2 R a^2 \sigma)$ is the plasma volume,

$R_p [= 2R\eta_{\parallel}/a^2\sigma\ (\eta_{\parallel} = \eta_{SPITZER} \times \alpha_{\eta})]$ is the plasma resistance,

$P_{oh} (= I_p^2 R_p)$ is the ohmic heating power,

$P_{ion} (= n_e n_o \langle\sigma v\rangle_{ion}\ kW_{ion}\ V_p)$ is the power lost in ionizing the hydrogenic fuel gas,

$P_{cx}(= 3/2\ n_e n_o \langle\sigma v\rangle_{cx}\ kT_i\ V_p)$ is the power loss associated with charge exchange events occurring between cold neutrals and warm ions, and

$P_{rad}[= 2 \times 10^{-12}\ n_e^{\ 2}\ \xi\ Ra^2\sigma\ L_z(T_e)]$ is the radiation power loss due to oxygen impurity.

The coronal equilibrium values for $L_z(T_e)$, the impurity emission rate per ion per free electron and $\langle Z_{oxy}\rangle$, the average charge state of an oxygen ion at a given T_e, are calculated from the model developed by Post et al.[26] In Eq. (8.2), f_R is the effective recycling coefficient and S_{EXT} is the particle source resulting from the ionization of cold hydrogenic neutrals introduced into the vacuum chamber. The parameter a_{eff} $(= a\sqrt{\sigma})$ is the effective circular plasma radius for an elongated plasma, $\eta_{\parallel}$ is the parallel plasma resistivity, α_η is an anomalous resistivity factor, and ξ $(= n_{oxy}/n_e)$ is the percentage of oxygen impurity in the plasma. The remaining parameters were defined earlier.

During the first 6 s of current startup, τ_E ranges from 2 ms to 0.4 s ($a \simeq 0.2$ m to 1.3 m, $\sigma = 1.0$ to 1.6, and $n_e \simeq 10^{19}\ m^{-3}$ to $3 \times 10^{19}\ m^{-3}$). Because the current rise time is much larger than the rapid energy and particle response time of the plasma, one can neglect the time derivatives in Eqs. (8.1) to (8.3), thereby obtaining the following quasi-steady-state particle and power balance equations:

$$n_o = (\langle\sigma v\rangle_{ion}\ \tau_p)^{-1} \tag{8.4}$$

$$n_e n_o \langle\sigma v\rangle_{ion} = \frac{n_e}{\tau_p}\ f_R + S_{EXT} \tag{8.5}$$

$$\frac{3.3 \times 10^{-9}\ \alpha_\eta\ \ell n\ \Lambda_{ei}\ Z_{eff}\ RI_p^{\ 2}}{a^2\sigma\ T_e^{\ 3/2}} + P_{RF} = 2.1 \times 10^5\ W_{ion}\ R$$

$$+ 3.2 \times 10^5 \left(\frac{\langle\sigma v\rangle_{cx}}{\langle\sigma v\rangle_{ion}}\right) T_e R + 2.0 \times 10^{-12}\ n_e^{\ 2}\ \xi Ra^2\sigma L_z(T_e)$$

$$+ 1.9 \times 10^6\ T_e R\ , \tag{8.6}$$

where

$$Z_{eff} = 1 + \xi\langle Z_{oxy}\rangle(\langle Z_{oxy}\rangle - 1) \ .$$

The explicit parametric dependence of each of the source and sink terms found in Eq. (8.3) is indicated in Eq. (8.6). Using Eq. (8.4), the neutral density has been eliminated in Eq. (8.6). Also, we have assumed that $T_e \simeq T_i$, and this assumption leads to pessimistic estimates of T_e during the initial stages of current rise when $\tau_{EQ}^{ei} = \tau_{ei}(m_i/m_e) \gtrsim 2\tau_E$ and $T_e > T_i$. At the end of current startup ($T_e \simeq 1$ keV, $n_e \simeq 3 \times 10^{19}$ m^{-3}, $a = 1.3$ m, and $\sigma = 1.6$), $\tau_{EQ}^{ei} \simeq 0.1\ \tau_E$, and the assumption is justified.

The second term on the right-hand side of Eq. (8.6) is the power loss due to charge exchange. With a purely inductive current startup, the plasma is initially cold ($T_e \simeq T_i \lesssim 2$ eV), and the mean free path for neutral penetration can be comparable to the plasma radius ($\lambda_{mfp} \gtrsim a_o \simeq 0.2$ m). At these low temperatures $\langle\sigma v\rangle_{cx}/\langle\sigma v\rangle_{ion} \simeq 1200$, indicating that charge exchange events can be a major energy loss mechanism early in the discharge.[35] However, with successful electron preheating ($T_e \simeq T_i \simeq 0.1$ keV, $n_e \simeq 10^{19}$ m^{-3}, and $a_o \simeq 0.2$-0.4 m), the plasma is much more effective in screening out neutrals ($\lambda_{mfp} < 5$ cm). The result is a significant reduction of charge exchange, as well as ionization and radiation losses.

Finally, because we treat n_e as an independent variable in these calculations, the quasi-steady-state value of n_o is determined from Eq. (8.4) for a given T_e. In turn, Eq. (8.5) can be used to estimate the required fueling rate, S_{EXT}. Hawryluk et al.[35] have pointed out, however, that control of S_{EXT} may be difficult because of the uncertainties in recycling and particle-induced desorption processes in the chamber wall.

8.2 CALCULATING THE APPLIED LOOP VOLTAGE AND ITS COMPONENTS

In estimating the applied voltage requirements, the controllable parameters are assumed to be the ECRH/ICRH power and the plasma current, density, and elongation. By specifying the plasma current, rather than

the applied voltage, the differential equation describing th ent evolution is used to determine the time history of the pla. voltage. Specifically, we have

$$V_\ell = V_{res} + V_{ind} = R_p I_p + \frac{d}{dt}(L_p I_p) \ , \tag{8.7}$$

where $V_{res} = P_{oh}/I_p$, and the plasma inductance is approximated by

$$L_p = \mu_o R \left[\ell n \left(\frac{8R}{a\sqrt{\sigma}} \right) + \frac{\ell_i}{2} - 2 \right] .$$

The dimensionless parameter ℓ_i is the flux-related definition of the internal inductance[36] and has a value of ~ 1 for broad current profiles.

During the expanding radius phase, the plasma inductance varies in accordance with the time dependent behavior of the major radius [Eq. (7.1)], minor radius [Eq. (7.4)], elongation, and dimensionless internal inductance. The general form for $I_p dL_p/dt$ can be written as follows:

$$I_p \dot{L}_p = I_p \left\{ \frac{\partial L_p}{\partial R} \dot{R} + \frac{\partial L_p}{\partial a} \dot{a} + \frac{\partial L_p}{\partial \sigma} \dot{\sigma} \right\} \ . \tag{8.8}$$

We have assumed $\dot{\ell}_i \approx 0$ since we maintain a uniform current profile during minor radius expansion and have no skin currents. With $\dot{a} = -\dot{R}$, Eq. (8.8) can be written explicitly as follows:

$$I_p \dot{L}_p = \mu_o I_p \left\{ \ell n \left(\frac{8R}{a\sqrt{\sigma}} \right) + A - 0.5 \right\} \dot{R} - \mu_o I_p \left\{ \frac{R}{2\sigma} \right\} \dot{\sigma} \ , \tag{8.9}$$

where A (= R/a) is the plasma aspect ratio. For a specified $\dot{I}_p$, $\dot{\sigma}$ and fixed q_I, the major radius compression rate is determined from

$$\dot{I}_p = 2 I_p \left\{ \frac{-\dot{R}}{R} + \frac{\dot{a}}{a} + \left(\frac{\sigma}{1 + \sigma^2} \right) \dot{\sigma} \right\} \ , \tag{8.10}$$

where

$$I_p(t) = \frac{2\pi[a(t)]^2 \; B(R_o) \cdot R_o}{\mu_o q_I [R(t)]^2} \left(\frac{1 + [\sigma(t)]^2}{2}\right)$$

and

$$\dot{a} = -\dot{R} \; .$$

8.3 RESULTS AND DISCUSSION

Starting with a reasonable time history for $I_p(t)$, Eqs. (8.6) and (8.7) have been used to study the time evolution of T_e, P_{oh}, V_{res}, and V_ℓ. The resistive flux expenditure during startup, $\Delta\phi_{res}$, has also been estimated by numerically integrating the area under the representative voltage curve.

Several expanding radius start-up cases have been generated to illustrate the sensitivity of the start-up requirements to variations in the initial minor radius, oxygen impurity content, and electron preheating level. The basic physics assumptions used in these cases include:

(1) flat temperature, density, and current density profiles during startup,

(2) uniform and total absorption of both ECRH and ICRH power by the plasma,

(3) $T_e \simeq T_i$ during the current rise phase,

(4) INTOR scaling for energy confinement,

(5) a relatively low $q_I \simeq 2.4$ corresponding to a flux-surface average value of $q_\psi = 3.2$,

(6) a controlled density buildup satisfying the "Murakami limit"[37,38] (a linear density ramp is assumed),

(7) a limitation on the maximum equilibrium and ballooning stability beta values specified at $\varepsilon\beta_p \simeq 0.5$ and $\beta_{crit} \simeq \varepsilon/q_I^2$, respectively,[38]

(8) uniform distribution of oxygen contaminate in those cases where impurity effects are examined,

(9) coronal equilibrium of oxygen impurity during startup, and

(10) a factor of 2 enhancement ($\alpha_\eta = 2$) in the Spitzer resistivity.

The results of our analysis are summarized in Table 4, and some typical examples are shown in Figs. 6-10. A varying major radius expansion (from $a_o = 0.2$ m) with rf assist and no impurities ($Z_{eff} = 1$) is shown in Fig. 6. Here the electrons have been preheated to ∿70 eV, a value which we believe is comparable to that already achieved in the ISX-B tokamak. By t = 50 ms, the plasma current has risen to ∿10 kA, and all of the physics constraints mentioned previously are satisfied. Supplemental ECRH (∿1 MW at 87 GHz) helps to maintain this electron temperature, as the plasma current and q_I-value evolve to their specified values of ∿42 kA and 2.36 at t = 200 ms. Over the next 5.8 s, the plasma current is ramped up linearly to the full ohmic heating current of 4.8 MA, while the plasma expands to full size (a = 1.3 m) and shape ($\sigma = 1.6$). Following 6 s of intense ICRF heating (50 MW at 54 MHz), the plasma enters the burn phase (lasting ∿100 s) where 180 MW of fusion power is sustained by 36 MW of ICRH (a plasma Q ∿ 5).[1]

Assessing the overall voltage and flux requirements during startup, Fig. 6 indicates that the resistive voltage reaches a maximum value (∿15 V) at t = 0.2 s. It then drops rapidly when the 5 MW of ECRH/ICRH power is applied during the expansion phase. The maximum V_ℓ is ∿21 V. During the burn phase, the loop voltage is decreased to ∿0.03 V, which is sufficient to maintain 5.4 MA of plasma current at 10 keV against resistive dissipation. The additional 0.6 MA of pressure driven current is produced during bulk heating and must be compensated for by current increases in the equilibrium field coils.[39] The inductive volt-seconds at full current are estimated to be $L_p I_p \simeq 54$ Wb assuming a flat current distribution. The accumulated loss of resistive volt-seconds during 6 s of current startup are calculated to be ∿10 Wb. Also shown in Fig. 6 is the behavior of the ohmic heating power during this period. Figure 6 indicates that the resistive heating power rises monotonically to about 0.6 MW at t = 0.2 s and about 4.0 MW at t = 6 s.

Table 4. Dependence of start-up requirements on initial plasma minor radius a_o, oxygen content n_{ox}/n_e, and electron temperature before current initiation $T_e(t = 0)$

Assumptions							
a_o (m)	0.2[a]	0.2[b]	0.2[c]	0.2[d]	0.4[e]	0.4[f]	0.4[g]
$\xi = n_{ox}/n_e$ (%)	0	3	3	3	0	3	3
$T_e(t = 0)$ (eV)	∿70	∿70	∿10	∿10	∿35	∿70	∿10
Requirements							
Maximum V_ℓ (V)	21	25	66	120	24	26	101
at time (s)	0.2	0.2	0.04	0.04	0.3	0.3	0.08
Resistive induction flux loss $\Delta\phi_{res}$ (Wb) at t = 6 s	10	18	19	42	10	17	22

[a]With electron preheating and P_{ECRH} = 1.0 MW for $0 \leq t \leq 0.2$ s.

[b]With preheating and a phased input of ECRH power given by $P_{ECRH} = 1.0(1 + 2.5\ t)$ MW for $0 \leq t \leq 0.2$ s.

[c]Same conditions as *b* but without electron preheating.

[d]Without electron preheating or rf assist during the current rise phase.

[e]With preheating and P_{ECRH} = 0.5 MW for $0 \leq t \leq 0.3$ s.

[f]With electron preheating and a phased input of ECRH power given by $P_{ECRH} = 1.0(1 + 2\ t)$ MW for $0 \leq t \leq 0.3$ s.

[g]Same conditions as *f* but without electron preheating.

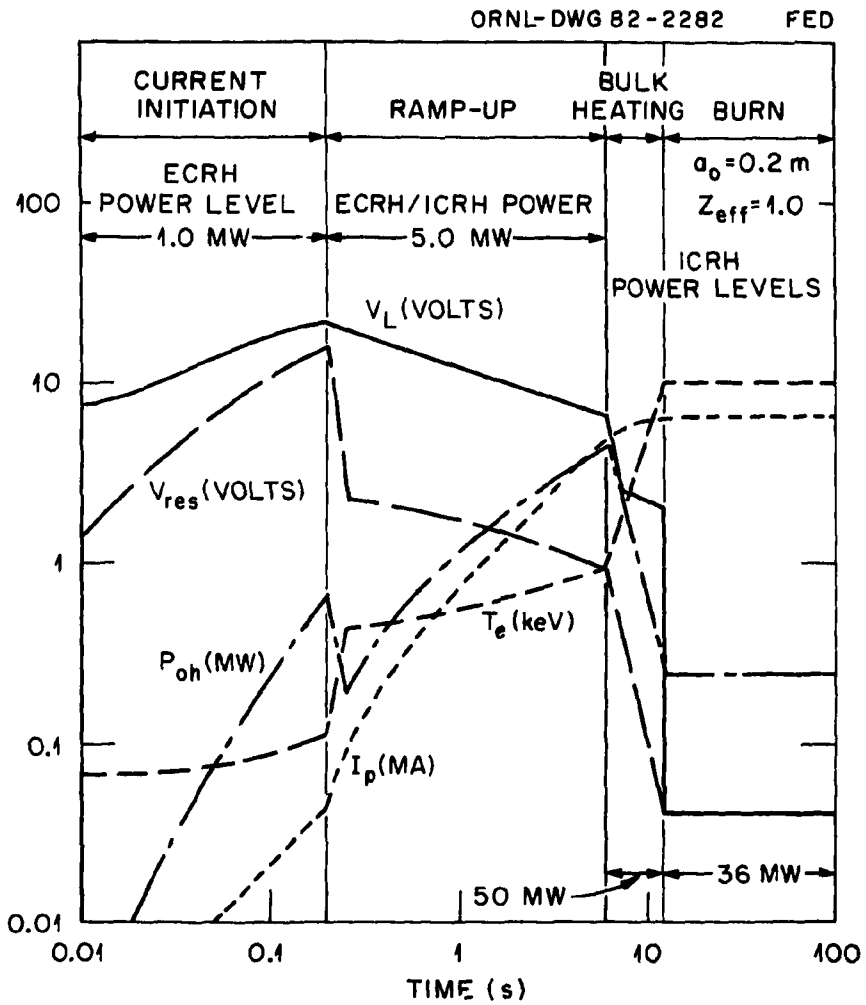

Fig. 6. Time evolution of key parameters in FED during an expanding radius startup (from an initial minor radius a_0 = 0.2 m) with electron preheating, rf assist and no oxygen impurity (Z_{eff} = 1).

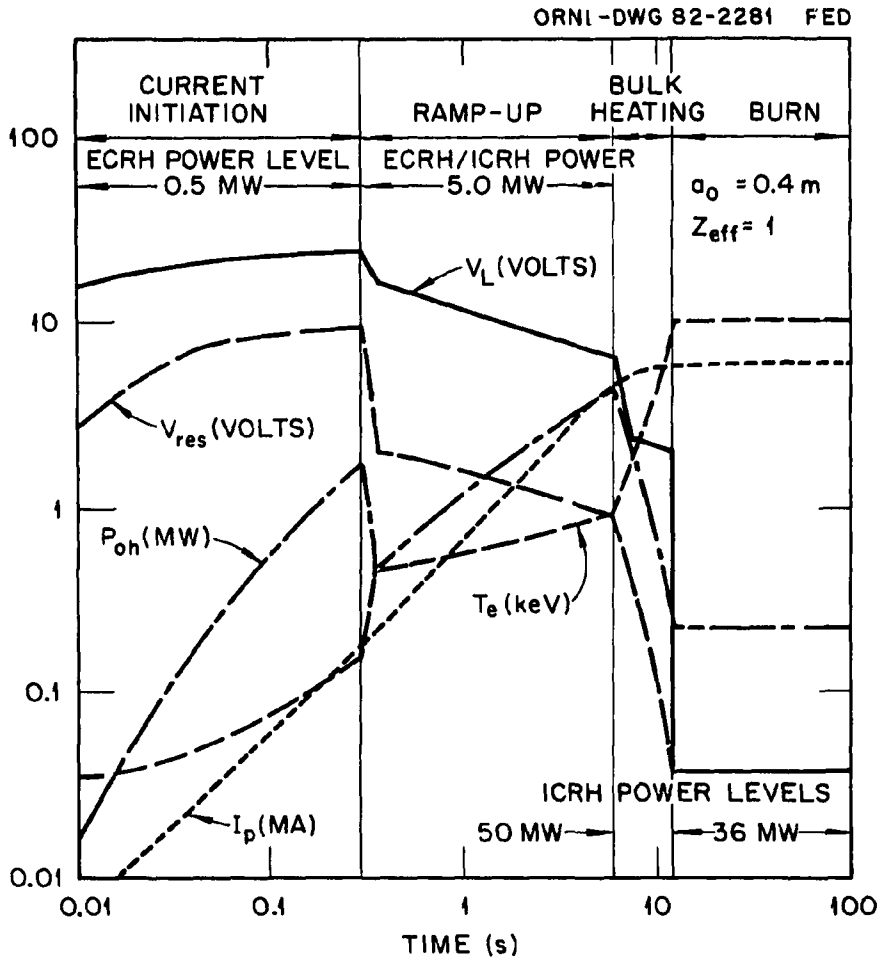

Fig. 7. Time evolution of same key parameters during an expanding radius startup of a clean (Z_{eff} = 1), 0.4 m minor radius plasma with preheating and rf assist.

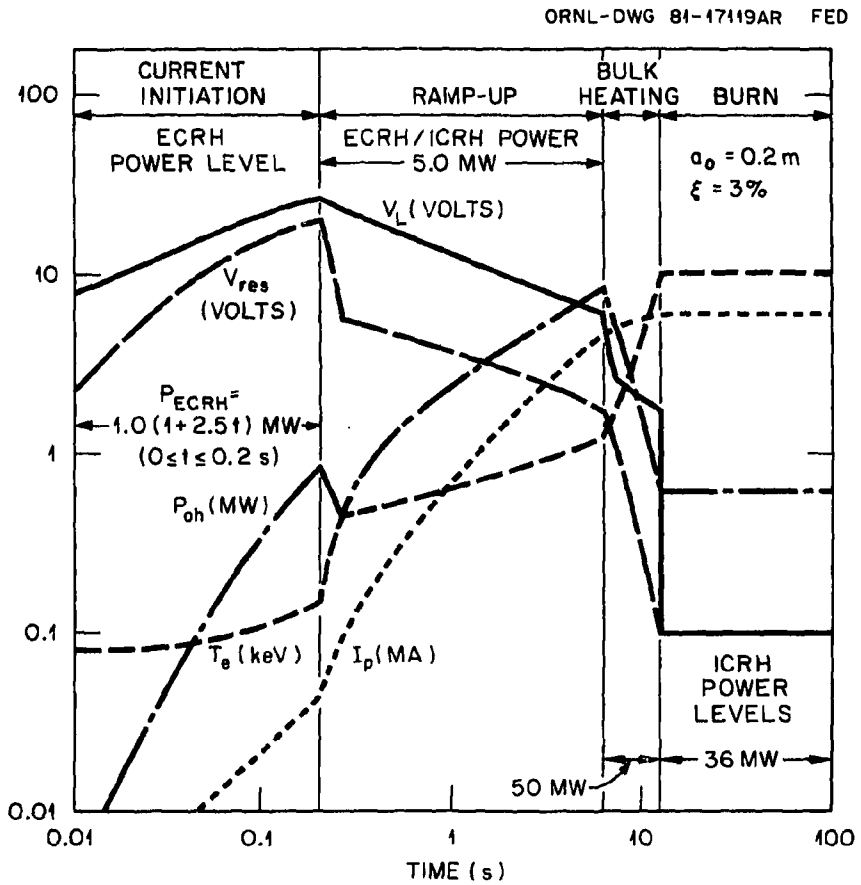

Fig. 8. Time evolution of key parameters in FED during an expanding radius startup (from a_o = 0.2 m) with electron preheating, rf assist and 3% oxygen impurity.

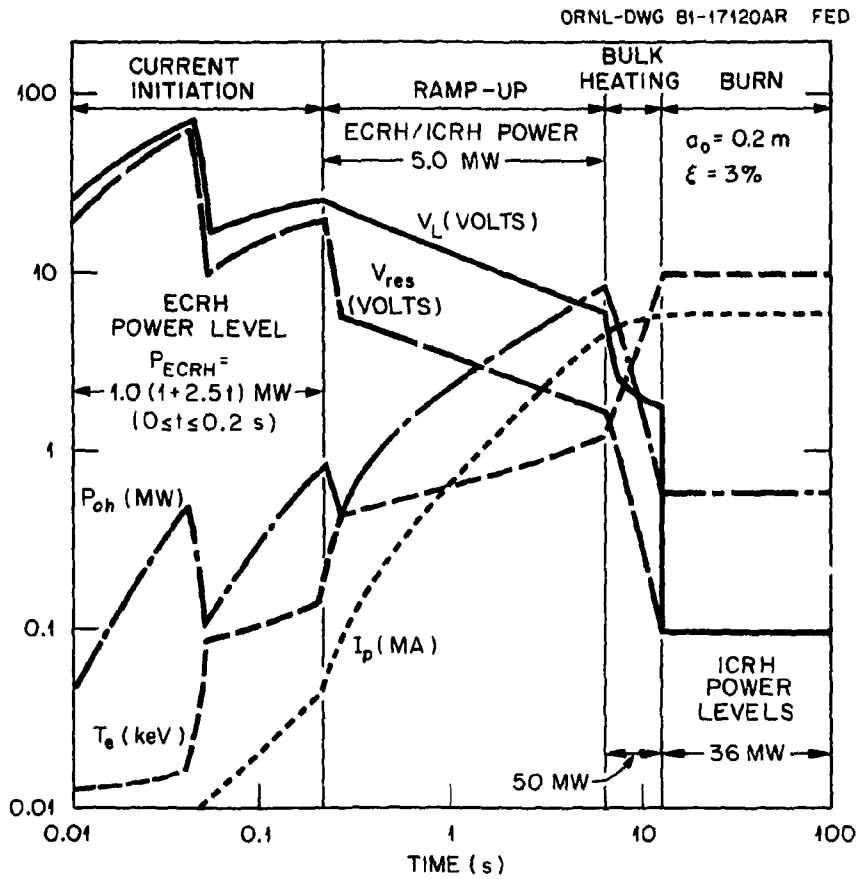

Fig. 9. Time evolution of same key parameters during an expanding radius startup as in Fig. 8 but without preheating. The time behavior is identical to that shown in Fig. 8 after 50 ms.

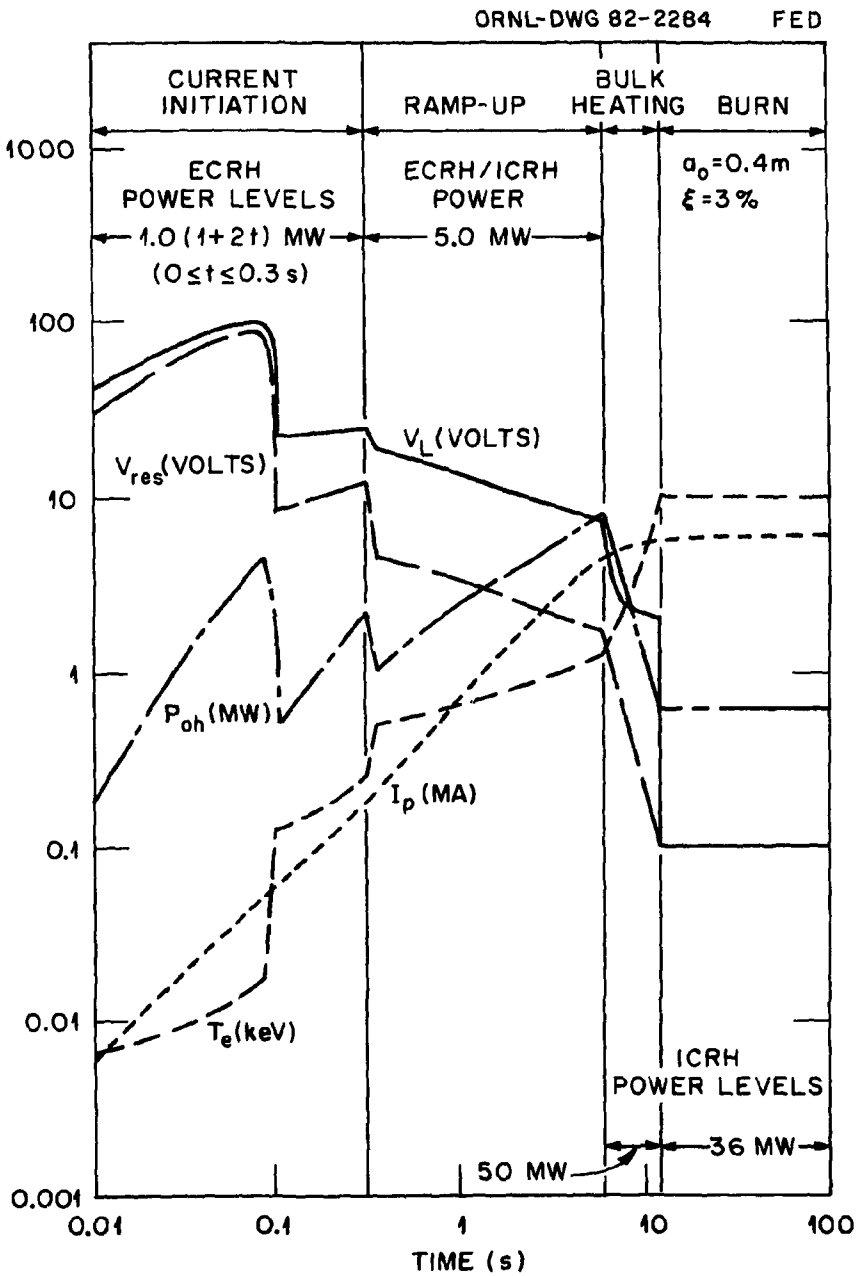

Fig. 10. Time evolution of key parameters in FED during an expanding radius startup (from a_o = 0.4 m) without electron preheating but with rf assist and 3% oxygen impurity.

For an initial minor radius of 0.4 m, Fig. 7 indicates that a maximum V_ℓ of $\sim$24 V is required in the absence of impurities. In going to a larger starting minor radius, it is necessary to increase the initial rate of current rise (from $\sim$0.2 MA/s to $\sim$0.6 MA/s) while reducing the level of electron preheating (from $\sim$70 eV to $\sim$35 eV). These changes minimize the time duration ($0 \leq t \leq 70$ ms) over which the various physics constraints cannot be satisfied. Preheating the plasma to just beyond the hydrogen ionization and radiation barrier ($\gtrsim$30 eV) enhances current penetration and reduces the possibility for skin current formation. A higher rate of current rise can also support increased plasma temperatures ($T_e \propto I_p^2/n_e a^2$ for fixed A and $T_e = T_i$) and more quickly satisfy the equilibrium and stability beta limits during current initiation.

With an oxygen impurity content of 3%, V_ℓ increases to $\sim$25 V for $a_o = 0.2$ m (Fig. 8) and $\sim$26 V for $a_o = 0.4$ m (Table 4). Because the $a_o = 0.4$ m case employs a greater rate of current rise during the initiation phase, it also requires a greater combined power input (1.6 MW of ECRH and 2.1 MW of P_{oh} at t = 300 ms) to minimize the resistive portion of the total loop voltage. In comparison, the $a_o = 0.2$ m case utilizes 1.5 MW of ECRH and $\sim$0.8 MW of P_{oh} at t = 200 ms.

Without electron preheating, small levels of oxygen impurity can dominate the plasma energy balance. At $T_e \simeq 20$ eV, $n_e \simeq 10^{19}$ m^{-3} and $\xi = 3\%$, oxygen's radiative power density is $\sim$0.27 MW/m^3. This large cooling rate ($\sim$1.26 MW for $a_o = 0.2$ m and $\sim$4.86 MW for $a_o = 0.4$ m) suppresses the electron temperature during the beginning stages of current initiation. Calculations for the $a_o = 0.2$ m (0.4 m) case indicate that if the electrons are not heated beyond 20 eV prior to current initiation, the maximum V_ℓ requirement increases to $\sim$65 V ($\sim$100 V), as indicated in Fig. 9 (10). An initiation voltage of $\sim$25 V would then fail to ramp up the plasma current as shown. This quantifies the importance of successful preheating to "burn through" the impurity radiation barrier prior to current initiation. The impact of no rf assist prior to and during plasma current rise is to raise further the maximum loop voltage (to >100 V for $a_o = 0.2$ m) and more than double the resistive flux consumption during the 6-s current start-up phase.

9. SUMMARY

We have developed a near classical particle and energy transport model for estimating the efficiency of electron heating in a currentless toroidal plasma. Magnetohydrodynamic (MHD) instabilities are presumed absent due to the presence of an ambipolar sheath and a conducting limiter and vacuum vessel that "short-circuits" potential vertical charge separation. The electrons are preferentially heated at the UHR by an extraordinary mode wave introduced from the high field side of the torus. The resulting loss of electrons via curvature and error field drifts leads to the formation of an ambipolar potential and poloidal $\vec{E}_{AMB} \times \vec{B}$ drift. This drift introduces an effective rotational transform which should improve particle confinement. Using this UHR heating model, we have reexamined the ISX-B experimental results and have found reasonably good agreement between our theoretical estimates and the diagnostic data.

On this basis, estimates for FED have been made assuming the presence of a low poloidal error field ($\sim$2 G), a plasma density of $n_e \simeq 10^{13}$ cm^{-3} and up to 3% oxygen content. Our results indicate that no more than 2 MW of ECRH power at $\sim$90 GHz is needed to achieve $T_e \lesssim 100$ eV in a volume of $\sim$5 m^3 near the UHR layer. Once the ECRH power burns through the oxygen radiation barrier in the UHR region, field cancelling coils would be used to eliminate the error field. This would allow the heating zone to increase to $\lesssim$30 m^3 in volume.

The ECRH power can be reduced to $\lesssim$1 MW during current initiation (with T_e maintained around 70 eV) without introducing serious skin currents. For an initial minor radius of 0.2 m (0.4 m), a time scale of about 0.2 s (0.3 s) is required to reach $I_p \simeq 0.04$ MA (0.18 MA) and $q_I \simeq 2.4$. The auxiliary heating power is then raised to about 5 MW (via a combination of ECRH/ICRH) to assist the relatively slow buildup of the plasma cross section to a = 1.3 m, $\sigma = 1.6$, and the plasma current to 4.8 MA in about 5.8 s.

Although a maximum V_ℓ close to 20 V has been indicated under relatively ideal conditions for $a_o = 0.2$ m, the V_ℓ requirement for FED is specified to be $\sim$25 V to account for uncertainties in impurity content and initial minor radius. A resistive induction flux capability of $\lesssim$20 Wb can also allow a slow current rise with up to 3% oxygen content.

The results of this study indicate that ECRH-assisted current startup is an effective method for reducing both the voltage and resistive flux requirements in FED. However, because this startup method has been examined on only one large tokamak (ISX-B), further experimental testing is required to demonstrate the continued viability of the rf-assisted startup process.

ACKNOWLEDGMENTS

The author (S.K.B.) would like to express his thanks to A. C. England, O. C. Eldridge, A. G. Kulchar, E. F. Jaeger, and W. A. Houlberg for helpful discussions and input on a variety of topics related to this work.

REFERENCES

1. The Fusion Engineering Device, Vol. II — Design Description, DOE/TIC-11600 (October 1981).
2. Y-K. M. Peng, S. K. Borowski, T. Kammash, Nucl. Fusion 16, 1489 (1978).
3. A. I. Anisimov, N. I. Vinogradov, B. P. Poloskin, Sov. Phys. — Tech. Phys. 18, 459 (1973); 20, 626 (1976); 20, 629 (1976).
4. V. V. Alikaev, Y. N. Dnestrovskii, V. V. Parail, G. V. Pereverzev, Sov. J. Plas. Phys. 3, 127 (1977).
5. O. C. Eldridge, W. Namkung, A. C. England, Electron Cyclotron Heating in Tokamaks, ORNL/TM-6052, Oak Ridge, Tennessee (1977).
6. B. Grek and M. Porkolab, Phys. Rev. Lett. 30, 836 (1973).
7. N. A. Krall and A. W. Trivelpiece, Principles of Plasma Physics, McGraw-Hill, New York, 409 (1973).
8. R. M. Gilgenbach et al., Nucl. Fusion 21, 319 (1981).
9. R. C. Isler et al., in Plasma Physics and Controlled Nuclear Fusion Research (Proc. 8th Int. Conf. Brussels, 1980) Vol. 1, IAEA, Vienna, 53 (1981).
10. D. J. Rose, M. Clark, Jr., Plasmas and Controlled Fusion, The MIT Press, Massachusetts Institute of Technology, Cambridge, Massachusetts, 201 (1961).
11. S. Yoshikawa, W. L. Harries, R. M. Sinclair, Phys. Fluids 6, 1506 (1963).
12. G. D. Hobbs, J. A. Wesson, Heat Transmission Through a Langmuir Sheath in the Presence of Electron Emission, CLM-R-61, Abingdon (June 1966); Plasma Phys. 9, 85 (1967).
13. A. C. England (Oak Ridge National Laboratory), private communication, 1981.
14. T. H. Stix, Phys. Fluids 14, 692 (1971).
15. D. G. Bulyginskii, V. S. Yuferev, E. V. Galaktionov, Sov. J. Plasma Phys. 3 (5), 528 (1977).
16. E. Hinnov, A. S. Bishop, H. Fullon, Jr., Plasma Phys. 10, 291 (1968).
17. V. E. Goiant, A. P. Zhilinsky, I. E. Sakharov, Fundamentals of Plasma Physics, John Wiley & Sons, New York, 307 (1980).

18. V. E. Golant, A. P. Zhilinsky, I. E. Sakharov, Fundamentals of Plasma Physics, John Wiley & Sons, New York, 278 (1980).
19. K. L. Wong, M. Ono, The Advanced Concepts Torus (ACT-1), Bull. Am. Phys. Soc. 24, 957 (1979).
20. V. D. Shafranov, Sov. At. Energy 18, 318 (1965).
21. V. S. Mukhovatov, V. D. Shafranov, Nucl. Fusion 11, 605 (1971).
22. B. H. Quon, R. A. Dandl, P. L. Colestock, H. Ikegami, Effects of Global Field Errors on ELMO Bumpy Torus, ORNL/TM-6075, Oak Ridge, Tennessee (1977).
23. L. S. Hall, Nucl. Fusion 17, 681 (1977).
24. A. E. Robson and P. C. Thonemann, Proc. Phys. Soc. 73, 508 (1959).
25. W. M. Stacey, Jr., Fusion Plasma Analysis, A Wiley-Interscience Publication, John Wiley & Sons, New York, 238 (1981).
26. D. E. Post, R. V. Jensen, C. B. Tarter, W. H. Grasberger, W. A. Lokke, Steady State Radiative Cooling Rates for Low Density High-Temperature Plasmas, PPPL-1532, Princeton, New Jersey (1977).
27. R. S. Granetz, I. H. Hutchinson, D. O. Overskei, Nucl. Fusion 19, 1587 (1979).
28. J. Hosea, D. Boyd, N. Bretz, R. Chrien, S. Cohen et al., in Plasma Physics and Controlled Nuclear Fusion Research (Proc. 8th Int. Conf. Brussels, 1980) Vol. 2, IAEA, Vienna, 95 (1981).
29. D. F. Duchs, H. P. Furth, P. H. Rutherford, Nucl. Fusion 12, 341 (1972).
30. W. A. Houlberg, A. T. Mense, S. E. Attenberger, Nucl. Fusion 20, 811 (1980).
31. Tokamak Fusion Test Reactor Reference Design Report, PPPL-1312, Princeton, New Jersey (1976).
32. ETF Design Center, ETF Interim Design Description Document, Oak Ridge, Tennessee (1980).
33. International Tokamak Reactor: Zero Phase, IAEA, Vienna (1980).
34. A. H. Spano, Nucl. Fusion 15, 909 (1975).
35. R. J. Hawryluk, J. A. Schmidt, Nucl. Fusion 16, 775 (1976).
36. R. J. Hawryluk, K. Bol, D. Johnson, Nucl. Fusion 19, 1519 (1979).
37. M. Murakami, J. D. Callen, L. A. Berry, Nucl. Fusion 16, 347 (1976).

38. C. A. Flanagan, D. Steiner, G. E. Smith, Initial Trade and Design Studies for the Fusion Engineering Device, ORNL/TM-7777, Oak Ridge, Tennessee (1981).

39. J. F. Clarke and D. J. Sigmar, Phys. Rev. Lett. 38, 70 (1977).